

1 **Impacts of Sea Ice Leads on Sea Salt Aerosols and Atmospheric Chemistry in the Arctic**

2 Erin J. Emme^{1,*}; Hannah M. Horowitz^{1,2,*}

Formatted: Centered

3
4 **¹Department of Civil and Environmental Engineering, University of Illinois Urbana-
5 Champaign, Urbana, Illinois, USA**

6 **²Department of Atmospheric Science, University of Illinois Urbana-Champaign, Urbana,
7 Illinois, USA**

8
9
10 **For submission to**

11 **Atmospheric Chemistry and Physics**

12 **October 9, 2024**

13 Formatted: Justified

14
15

*Corresponding authors: Erin J. Emme, emme2@illinois.edu, and Hannah M. Horowitz,
16 hmhorow@illinois.edu.

17
18

19 **Impacts of Sea Ice Leads on Sea Salt Aerosols and Atmospheric Chemistry in the Arctic**

20 Erin J. Emme¹, Hannah M. Horowitz^{1,2}

21 ¹Department of Civil and Environmental Engineering, University of Illinois at Urbana-
22 Champaign, Urbana, 61801, USA

23 ²Department of Atmospheric Sciences, University of Illinois at Urbana-Champaign, Urbana,
24 61801, USA

25 **Correspondence to:** Erin J. Emme (emme@illinois.edu) and Hannah Horowitz
26 (hmhorow@illinois.edu)

27
28 **Abstract.** ~~Sea salt aerosols (SSA) alter Arctic climate through interactions with radiation and~~
29 ~~clouds.~~ The processes contributing to Arctic cold season (November-April) sea salt aerosols
30 (SSA) remain uncertain. Observations from coastal Alaska suggest emissions from open leads in
31 sea ice, which are not included in climate models, may play a dominant role. Their Arctic-wide
32 significance has not yet been quantified. Here, we create an emissions parameterization of SSA
33 from leads by combining satellite data of lead area (the AMSR-E product) and a chemical
34 transport model (GEOS-Chem) to quantify pan-Arctic SSA emissions from leads during the cold
35 season from 2002-2008 and predict their impacts on atmospheric chemistry. evaluating the
36 results of our simulated SSA against in-situ observations. The AMSR-E product detects large
37 leads with certainty (>3 km in size) and hence our study is limited to quantifying emissions from
38 large leads. Lead emissions vary seasonally and interannually. Simulated t Total monthly SSA
39 emissions increase by 1.1-1.8% ($\geq 60^\circ\text{N}$ latitude) and 5.6-7.5-8.4% ($\geq 75^\circ\text{N}$) for the 2002-2008
40 cold season. ~~The AMSR-E product detects at least 50% of total lead area as compared to optical~~
41 ~~MODIS satellite images.~~ SSA concentrations increase primarily at the location of leads, where
42 standard model concentrations are low. GEOS-Chem overestimates SSA concentrations at Arctic
43 sites compared to ground observations even when lead emissions are not included, suggesting
44 underestimation of SSA sinks and/or uncertainties in SSA emissions from blowing snow and open
45 leads ocean. Multi-year monthly mean surface bromine atom (Br) concentrations increase 2.8-
46 8.8% due to SSAs from leads for the 2002-2008 cold season. Changes in ozone concentrations
47 are negligible. While leads contribute <10% to Arctic-wide SSA emissions in the years 2002-2008,
48 these emissions occur in regions of low background aerosol concentrations. Leads ~~are also~~
49 ~~expected to~~ may increase in frequency under future climate change, which could increase SSA
50 emissions from leads. ~~Thus, lead SSA emissions could have significant impacts on Arctic climate.~~

51
52 **Short Summary**

53 There is uncertainty in the sources of Arctic cold season (November-April) sea salt aerosols.
54 Using a chemical transport model and satellite observations, we quantify Arctic-wide sea salt
55 aerosol emissions from fractures in sea ice, called open sea ice leads, and their atmospheric
56 chemistry impacts for the cold season. We show sea ice leads contribute to Arctic sea salt
57 aerosols and bromine, especially in under-observed regions.

58

59 1. Introduction

60

61 Sea salt aerosols (SSA) affect Arctic climate by scattering incoming solar radiation and acting as
62 cloud condensation nuclei and ice nuclei (DeMott et al., 2016; Pierce and Adams, 2006; Quinn et
63 al., 1998). In the Arctic, these processes are relevant during the fall and spring, but negligible
64 during polar night, when there is no sunlight. Long-term measurements have shown that peak
65 SSA concentrations in the Arctic occur during the cold season (Leaitch et al., 2018; Quinn et al.,
66 2002; Schmale et al., 2021). However, the sources and mechanisms of cold season SSA
67 emissions are uncertain, which hinders atmospheric chemistry and climate models from
68 accurately representing polar regions. Recent observations from Utqiaġvik, Alaska have
69 suggested that open leads, or open sea ice fractures, are an important source of cold season
70 SSA emissions (Kirpes et al., 2019; May et al., 2016). Climate change has impacted the Arctic by
71 rapidly decreasing sea ice age and thickness (Intergovernmental Panel On Climate Change,
72 2023; Sumata et al., 2023; Vaughan et al., 2013), and future projections indicate this will continue
73 (Intergovernmental Panel On Climate Change, 2023), suggesting the amount of open leads will
74 increase in the future due to thinner ice that is prone to fracture. More work is needed to discern
75 the Arctic-wide importance and impacts of SSA emissions from sea ice leads ("lead emissions")
76 on atmospheric chemistry and climate. By combining satellite observations and chemical
77 transport modeling, we quantify the significance and impacts of lead emissions on atmospheric
78 concentrations of SSA and bromine and evaluate simulated SSA against in-situ observations.

79

80 While global models have not yet included SSA emissions from leads, several observational
81 studies largely based in Utqiaġvik, Alaska suggest have investigated the importance of emissions
82 of SSA from leads may be important. ~~lead-based SSA.~~ Key early observations in the 1970s in
83 Utqiaġvik, ~~Alaska~~, by Scott & Levin (1972) and Radke et al. (1976) demonstrated an increase in
84 sodium-containing particles in the presence of open water leads. ~~Since then, more recent~~
85 measurement studies have quantified SSA emissions from leads. Nilsson et al. (2001) estimate
86 that leads contribute an order of magnitude less than the open ocean to the Arctic SSA flux during

Formatted: Font: 11 pt

Formatted: Font: 11 pt

Formatted: Font: 11 pt

Formatted: Font: 11 pt

Field Code Changed

Formatted: Font: 11 pt

Field Code Changed

Formatted: Font: 11 pt

Formatted: Justified

Field Code Changed

Field Code Changed

87 ~~the summer months.~~ ~~More recently,~~ A multi-year study of observed SSA at Utqiaġvik (May et
88 al., 2016), conducted over all seasons, found that leads are a significant contributor to SSA
89 through wind-driven production, increasing the supermicron range in particular, but again to a
90 lesser extent than wind-driven production from the open ocean.; ~~Nilsson et al. (2001) estimate~~
91 ~~that leads contribute an order of magnitude less than the open ocean to the Arctic SSA flux during~~
92 ~~the summer months.~~ ~~Held et al. (2011) found that leads do not contribute significantly to Arctic~~
93 ~~summertime SSA under low wind speeds below the threshold for open sea spray aerosol~~
94 ~~production ($\sim 4 \text{ m s}^{-1}$).~~ ~~Kirpes et al. (2019) identified SSA produced by local leads as the dominant~~
95 ~~aerosol source in the coastal Alaskan Arctic during winter months.~~ ~~In addition,~~ Willis et al. (2018)
96 suggest that lead emissions are more important in winter and early spring as winds over the
97 Northern oceans are at their highest. Kirpes et al. (2019) also convey the importance of
98 seasonality, identifying SSA produced by local leads as the dominant aerosol source in the
99 coastal Alaskan Arctic during winter months. Chen et al. (2022), focusing on the spring, also
100 ~~shows in a recent study during the month of April~~ at Utqiaġvik, that leads were present locally
101 throughout the study, and ~~that they~~ contributed to sea spray aerosol production. As ground-based
102 observations in the Arctic are mainly limited to coastal stations, such as Utqiaġvik, it is difficult to
103 estimate the significance and impacts of lead emissions over the entire Arctic. Representing
104 Arctic-wide emissions from leads in a global chemical transport model, especially during the cold
105 season, will help discern whether lead emissions and their impacts on atmospheric chemistry are
106 significant enough to warrant inclusion in chemistry as well as climate models.

Field Code Changed

107
108 Other modeling studies in the Arctic and observations primarily from Antarctica suggest blowing
109 snow, ~~where saline snow over sea ice is swept up by wind,~~ is a potential major contributor of cold
110 season SSA in polar regions. Blowing snow SSA comes from saline snow over sea ice that is
111 swept up by wind; the snow becomes salty through the upward movement of brine from sea ice
112 to the snow surface, incorporation of frost flowers, and deposition of SSA from the nearby open
113 ocean (Domine et al., 2004). In two chemical transport models, the inclusion of additional SSA
114 emissions from blowing snow brought simulated SSA mass concentrations closer to what was
115 observed (Confer et al., 2023; Huang et al., 2018; Huang and Jaeglé, 2017; Rhodes et al., 2017).
116 Other potential sources of cold season SSA, such as frost flowers, have been found to be
117 insignificant (Alvarez-Aviles et al., 2008; Roscoe et al., 2011; Yang et al., 2017). Incorporating
118 blowing snow SSA emissions into models has shown how missing sources of SSA in the Arctic
119 can have a significant impact on atmospheric chemistry: for example, ~~(Huang et al., 2020) show~~
120 bromine released by blowing snow impacts modeled springtime bromine activation and ozone

Formatted: Justified

Formatted: Font: (Default) Arial, 11 pt

Field Code Changed

121 ~~depletion events. The strong observational evidence that leads contribute to cold season SSA~~
122 ~~and the impact of blowing snow SSA on modeled Arctic atmospheric chemistry suggests there is~~
123 ~~a emphasizing the~~ need to assess the potential impacts of lead emissions, which are currently
124 missing from global chemistry and climate models. One study incorporated SSA emissions from
125 leads in a chemical transport model (WRF-Chem), but the study was limited to the 400 km² area
126 surrounding Utqiagvik, Alaska and used ERA-5 reanalysis sea ice fraction to define the presence
127 of leads (Ioannidis et al., 2023)(~~Ioannidis et al., 2022~~). They find open leads are the primary
128 source of fresh and aged SSA in Utqiagvik, Alaska during the cold season, consistent with the
129 observational analysis by May et al. (2016) and Kirpes et al. (2019).

Formatted: Font: (Default) Arial, 11 pt

130
131 SSA play a critical role in Arctic tropospheric chemistry. SSA debromination is the main global
132 source of reactive bromine in the troposphere (Wang et al., 2021). Reactive bromine chemistry
133 has been attributed to the rapid depletion of ozone in the Arctic springtime, which reaches a
134 maximum in March-April (Simpson et al., 2007). In particular, bromine atom (Br) is key to these
135 ozone depletion events; it is produced through the photolysis of Br₂, which is sourced from SSA
136 debromination and snowpack chemistry (Abbatt et al., 2012; Dibb et al., 2010; Pratt et al., 2013;
137 Stutz et al., 2011). Swanson et al. (2022) show improved springtime model-observation
138 agreement of BrO by including a snowpack photochemistry mechanism based on multiple field
139 observations in a global chemical transport model. While on a global scale, reaction of OH with
140 other SSA-sourced bromine species can also produce Br (Wang et al., 2021), this is minor in polar
141 regions due to low OH concentrations. Br rapidly depletes ozone through heterogeneous
142 reactions, which produces BrO that can photolyze to reform Br, creating a catalytic ozone-
143 depletion cycle (Simpson et al., 2007).

Field Code Changed

Field Code Changed

Field Code Changed

144
145 Here, we estimate the pan-Arctic contribution of leads to total SSA emissions during the cold
146 season for the years 2002-2008, by using satellite observations of lead area to parameterize lead-
147 based SSA production in the global chemical transport model GEOS-Chem. We evaluate
148 simulated SSA concentrations against observations and predict the impacts of lead SSA
149 emissions on atmospheric chemistry, including concentrations of Br and ozone.

Formatted: Justified

150

151 2. Methods

152

153 2.1 Satellite Data of Lead Area Fractions

154

155 In this study, we use satellite data of lead area fractions to inform the GEOS-Chem chemical
156 transport model (next section) of where leads are present. The Advanced Microwave Scanning
157 Radiometer-Earth Observation System (AMSR-E) sensor aboard NASA's Aqua satellite
158 recorded brightness temperatures from Earth from 2002-2011 at six different frequencies
159 (<https://www.cen.uni-hamburg.de/en/icdc/data/cryosphere/lead-area-fraction-amsre.html>)
160 (Integrated Climate Data Center (ICDC) et al., n.d.), which are converted to lead area fractions
161 following the algorithm of Röhrs and Kaleschke (2012). This method of detection can only be
162 applied to the Arctic freezing season (November-April) due to surface melt of the sea ice modifying
163 the sea ice emissivity from May-October, which affects the lead detection algorithm. Daily data is
164 available at 6.25 km horizontal resolution, as the algorithm is not limited by cloud cover. The
165 AMSR-E satellite data is regridded to 0.5°x0.625° from 6.25x6.25 km using a distance-weighted
166 average remapping for consistency with the emission model's resolution (see Sect. 2.2 below for
167 model details). For the rare individual days with missing data in the dataset (0.8%), we use the
168 average lead area fraction for that month. The lead area fraction includes open water leads and
169 thin ice-covered leads 3 km and wider. The data spans latitudes 41° to 90°N, though a majority
170 of Arctic sea ice lies above 60°N and leads are therefore unlikely to be present at lower latitudes.

171
172 We ~~choose~~ use the AMSR-E lead area product for this study as it avoids cloud interference when
173 detecting leads and provides nearly consistent daily resolution. A limited quantitative validation
174 by Röhrs and Kaleschke (2012) of qualitatively validated this lead dataset against one day (March
175 21, 2006) of the AMSR-E product against the Moderate Resolution Image Spectroradiometer
176 (MODIS) showed and found that more than 50% of the total lead area visible in 500 m MODIS
177 images was detected in the AMSR-E product. Leads greater than 3 km in size ("large leads")
178 were detected with certainty for the AMSR-E product (Röhrs and Kaleschke, 2012), so our results
179 effectively estimate emissions from large leads only. However, the MODIS sea surface
180 temperature product is constrained to clear sky conditions, with Arctic winter conditions affecting
181 cloud identification techniques (Hoffman et al., 2022); it is also difficult to discern the thermal
182 contrast and shape of cloud edges and shadows from the temperature contrast of leads (Reiser
183 et al., 2020).

184 2.2 GEOS-Chem: global chemical transport model

185
186
187 Here we use the 3-D atmospheric transport model GEOS-Chem (geos-chem.org) version 13.2.1
188 (<https://doi.org/10.5281/zenodo.5500717>) (~~Community, 2021~~). Within GEOS-Chem, the

Formatted: Font: (Default) Arial, 11 pt

Formatted: Justified

Field Code Changed

189 Harmonized Emissions Component (HEMCO) computes emissions for different sources, regions,
190 and species (Keller et al., 2014). GEOS-Chem and HEMCO are driven by Modern-Era
191 Retrospective Analysis for Research and Applications (MERRA-2) (Gelaro et al., 2017)
192 meteorological fields from the NASA Global Modeling and Assimilation Office (GMAO), which is
193 reanalysis meteorological data assimilated from various observational sources (i.e., satellite,
194 aircraft campaigns, and ground stations) providing variables such as temperature, wind,
195 precipitation, and humidity. GEOS-Chem represents one-way interactions between the MERRA-
196 2 meteorology and chemical constituents, meaning the meteorological conditions can affect the
197 concentration of chemical species but not vice versa.

198
199 SSA emissions calculations for the open ocean use a wind- (Gong, 2003; Monahan et al., 1986)-
200 and sea-surface-temperature-dependent (Jaeglé et al., 2011) source function. In polar regions,
201 SSA emissions from blowing snow are also included (Huang and Jaeglé, 2017). SSA have two
202 size bins: coarse mode (SALC; $r = 0.5$ to $10 \mu\text{m}$) and accumulation mode (SALA; $r = 0.1$ to 0.5
203 μm). For gas and aerosol species, wet deposition (both rain and snow) includes washout and
204 rainout in convective and large-scale stratiform precipitation (Amos et al., 2012; Liu et al., 2001;
205 Wang et al., 2014). From November to April in the Arctic, wet deposition is mainly in the form of
206 snow (Screen and Simmonds, 2012). Dry deposition of gas and aerosol species follows a
207 resistance-in-series approach, and includes gravitational settling of sea salt (Jaeglé et al., 2011;
208 Pound et al., 2020; Wang et al., 1998; Zhang et al., 2001). Coupled gas- and multiphase-reactive
209 halogen chemistry, including sea salt debromination, acid displacement, and photolysis and
210 oxidation of gas-phase inorganic bromine and chlorine species, is described in Wang et al. (2021).
211 This version of GEOS-Chem does not include snowpack chemistry as a source of reactive
212 bromine in the standard model.

213
214 We parameterize SSA emissions from leads with the same function as the open ocean emissions
215 from Jaeglé et al. (2011) (Eq. (S.1) in the Supplemental Information (SI)), scaled by the fractional
216 area of leads in each grid cell from the AMSR-E satellite data. The Jaeglé et al. (2011) function is
217 empirically derived to best match global observations in GEOS-Chem. We assume that leads emit
218 SSA at an equal rate as a function of lead area. The AMSR-E satellite data is regridded to
219 $0.5^\circ \times 0.625^\circ$ from 6.25×6.25 km using a distance-weighted average remapping. This lead
220 emissions parameterization is a unique wind- and SST-dependent source function for calculating
221 lead emissions, driven by satellite observations defining the presence of leads. Nilsson et al.
222 (2001) derive an empirical lead emissions flux with an exponential dependence on windspeed

Formatted: Justified

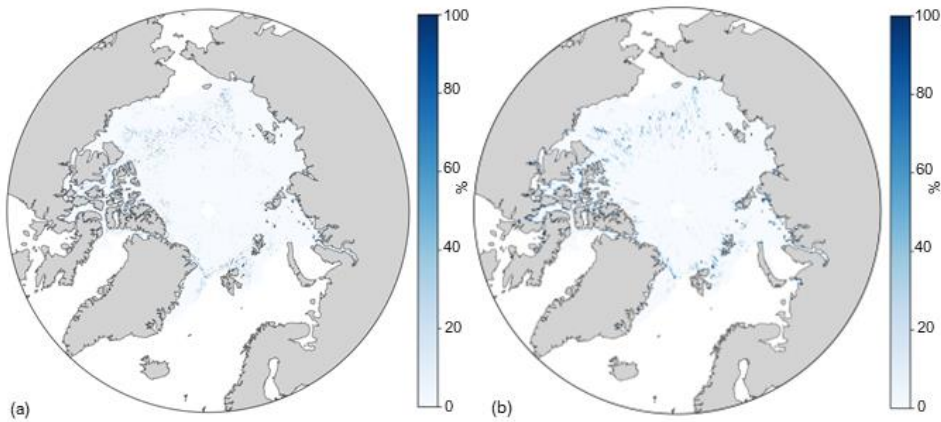
Formatted: Font: (Default) Arial

223 and no consideration of SST (Eq. (S.2) in SI), and for a given windspeed find lower emissions
224 from than the open ocean due to a lower fetch. Ioannidis et al. (2022) use a similar source function
225 to this study which has slight differences in the exact SST and wind speed dependencies
226 compared to GEOS-Chem; emissions from leads follow the same function as the open ocean and
227 they define the presence of leads as the fraction of each grid cell which is ice free. Figure 1
228 shows an example of the daily temporal frequency and spatial resolution of the AMSR-E satellite
229 data (both the raw (a) and regrided (b)) used to drive the model.

230

Formatted: Justified

AMSR-E Lead Area Fraction



231

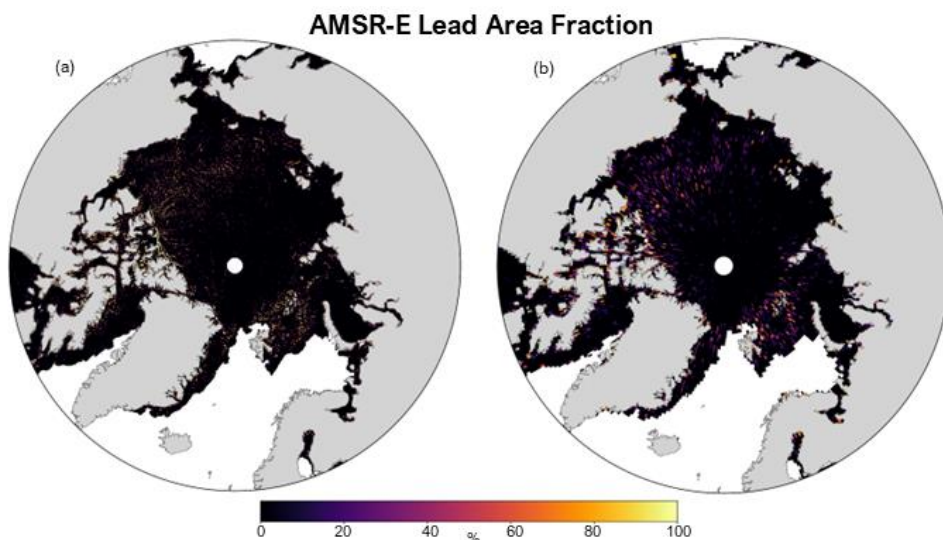


Figure 1- Map of AMSR-E daily lead area fraction in percent (%) for November 1, 2002, both raw (6.25-km resolution) (a) and re-gridded (0.5°x0.625° resolution) (b).

~~We perform simulations to quantify lead emissions and their impact on atmospheric chemistry at the highest global horizontal (2° latitude x 2.5° longitude) and vertical (72 vertical levels) resolution. We first calculate SSA emissions at the highest resolution of HEMCO (0.5°x0.625°), which is the native resolution of MERRA-2. Two sets of emissions are calculated: (1) the standard emissions only (i.e., open ocean and blowing snow SSA emissions, the “standard” case); (2) SSA emissions with lead emissions added (“standard + leads” case). Each set of eEmissions are then implemented separately into GEOS-Chem “offline” to ensure total SSA emissions are properly scaled and distributed and not influenced by the resolution-dependence of the wind speed (Lin et al., 2021). GEOS-Chem is run at the highest global horizontal (2° latitude x 2.5° longitude) and vertical (72 vertical levels) resolution. We calculate two sets of emissions for two simulations: (1) the standard emissions only (i.e., open ocean and blowing snow SSA emissions, the “standard” case); (2) SSA emissions with lead emissions added (“standard + leads” case). The absolute difference between the standard + leads and standard simulations two is the change in SSA emissions or concentration from leads, and we present the percent change due to leads (%) as calculated with Eq. (1).~~

252
$$\text{Percent change due to leads (\%)} = 100 \times \frac{(\text{Standard+leads})_{\text{simulation}} - (\text{Standard})_{\text{simulation}}}{(\text{Standard})_{\text{simulation}}} \times 100$$

253 (1)

254

255 Simulations are performed for the years 2002-2008, when there is overlap between the AMSR-E
256 satellite data and available observed Arctic SSA concentrations at multiple sites, following one
257 year of initialization. Because satellite observations of lead area fractions begin November 1,
258 2002, we initialize the standard + leads case for GEOS-Chem with standard + leads SSA
259 emissions for one year (November 1, 2002 to November 1, 2003) and then start the simulation
260 for analysis on November 1, 2002, with the spun-up November 1, 2003, initial conditions. For the
261 standard case, the initialization year begins November 1, 2001. For both cases, we simulate SSA
262 concentrations, evaluate against observed concentrations, and assess the impacts of additional
263 lead emissions on atmospheric chemistry. This includes analysis of the change in atmospheric
264 concentrations of bromine atom (Br) and ozone (O₃). For model evaluation, GEOS-Chem does
265 not track sodium (Na⁺) content for SSA, so we convert simulated SSA to Na⁺ mass concentrations
266 using a factor of $\frac{1}{3.256}$, which is based on the mass ratio of Na⁺ in seawater (Confer et al., 2023;
267 Huang and Jaeglé, 2017; Riley and Chester, 1971).

268

269 2.3 In-Situ Observations of Arctic Sea Salt Aerosol Concentrations

270

271 We evaluate simulated concentrations of SSA from GEOS-Chem, converted to Na⁺
272 concentrations, against in situ observations of Na⁺ concentrations at ~~43~~ Arctic sampling sites:
273 Utqiaġvik, Alaska (71.3°N, 156.6°W; 11m a.s.l.) (Quinn et al., 2002); Zeppelin Mountain, Svalbard,
274 Norway (78.9°N, 11.9°E; 475m a.s.l.) (World Meteorological Organization (WMO), 2003); Alert,
275 Nunavut, Canada (82.5°N, 62.5°W; 210m a.s.l.) (World Meteorological Organization (WMO),
276 2003); Pallas (Matorova), Helsinki, Finland (68 °N, 24.24 °E; 340m a.s.l.) (Salmi, 2018). These
277 observations are available for the time period of this study (November-April from 2002-2008,
278 except for Pallas station, 2003-2008). In winter months, ~~these the~~ Utqiaġvik, Zeppelin, and Alert
279 coastal sites border mostly ice-covered ocean (Huang and Jaeglé, 2017). At Utqiaġvik, mass
280 concentrations of Na⁺ for submicron and supermicron aerosols are separated, while the other two
281 sites measure the total mass concentration without size distinction. The Na⁺ mass concentrations
282 are determined from ion chromatography with uncertainties of 5-11%, or an absolute uncertainty
283 of 0.01 µg/m³ (Quinn et al., 2000; World Meteorological Organization (WMO), 2003). The aerosol

Field Code Changed

Formatted: Justified

Formatted: Font: (Default) Arial, 11 pt

284 sampling frequency is daily at Zeppelin, ~~and~~ Utqiagvik (submicron), ~~and~~ Pallas and weekly at Alert
285 and Utqiagvik (supermicron).

286

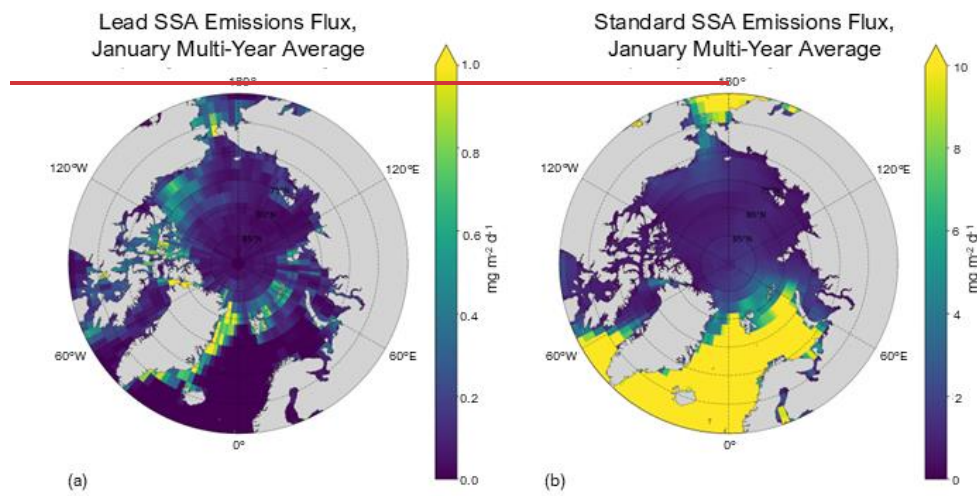
Formatted: Justified

287 3. Results

288

289 3.1 Emissions of Sea Salt Aerosols from Leads

290



291

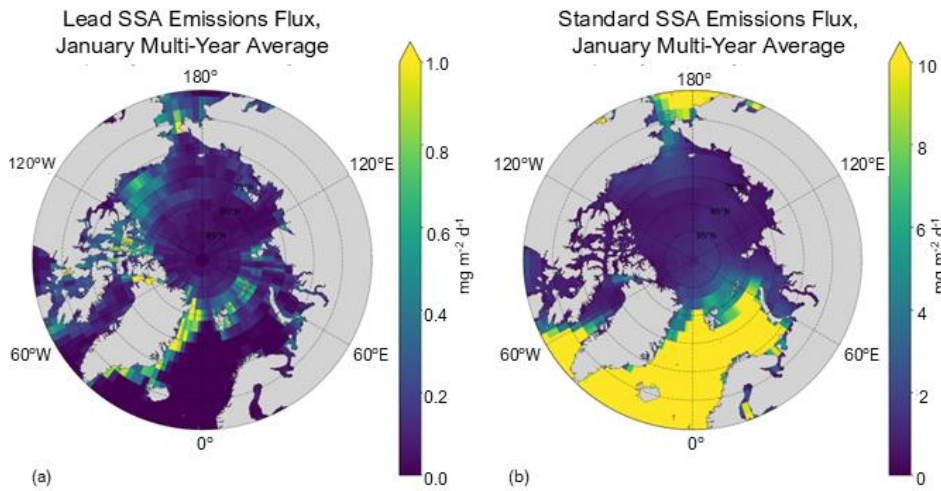


Figure 2- Total (coarse + accumulation mode) lead SSA emissions (a) and standard SSA emissions (b), averaged over 2002-2008 for January. Note the difference in magnitude of the colorbar of (a) and (b).

Figure 2a shows the spatial distribution of multi-year (2002-2008) average lead emissions for the month of January, which is a climatology based on model simulations that use daily resolution lead data (e.g., Fig. 1). We focus Figs. 2 and 4 on the month of January as [an example. January](#) ~~it is tied for highest lead emissions for latitudes 60°N and greater and second highest for latitudes 75°N and greater (Table 1), and also has the second largest multi-year average lead area (see Fig. S.3b in SI) is the month with the highest relative increase in SSA emissions for latitudes 75°N and higher (Table 1).~~ Alongside Fig. 2a is the standard model, which includes open ocean and blowing snow emissions (Fig. 2b; see Sect. 2.2). Total emissions are resolution independent and are shown in Fig. 2 for the 2.0°x2.5° resolution of the online atmospheric chemistry simulation. We find the lead emissions ~~and lead area are spatially consistent are concentrated in regions where leads are present (Figs. 1 and 2a)~~ and occur in regions where the standard SSA emissions are low (e.g., in the Greenland Sea and parts of the Barents Sea). The percent change in SSA emissions due to leads (calculated with Eq. (1)) is detailed in Table 1 ~~and Fig. 2~~; Figs. 4, 5, and S.4 show the percent change in SSA concentration due to leads. Generally, emissions tend to be higher from 70° to 80° N and more concentrated [within the Bering Strait, Nares Strait, Wynnaiatt](#)

Formatted: Centered

Formatted: Justified

Formatted: Font: Not Bold

Formatted: Font: Not Bold

312 Bay in the Canadian archipelago, and the eastern Greenland Sea off the coasts of Northern
 313 Canada and Greenland, as opposed to off the coast of Northern Russia and Europe. Month to
 314 month, regions where emissions are higher remains similar while the magnitude varies (see Fig.
 315 S.1 in SI).

316

Month	Multi-Year (2002-2008) Average Standard Emissions [Gg]		Multi-Year (2002-2008) Average Lead Emissions [Gg] (and corresponding Monthly Percent Change in SSA Emissions due to Leads)	
	≥60°N	≥75°N	≥60°N	≥75°N
November	7800 ± 1000	610 ± 210	82 ± 0.14 (1.1% ± 0.14%)	42 ± 0.13 (6.97% ± 0.13%)
December	8700 ± 1400	640 ± 140	110 ± 0.20 (1.23% ± 0.20%)	48 ± 0.32 (7.56% ± 0.32%)
January	8400 ± 1100	670 ± 290	110 ± 0.10 (1.34% ± 0.10%)	46 ± 0.15 (6.98% ± 0.15%)
February	6700 ± 850	510 ± 90	100 ± 0.11 (1.56% ± 0.11%)	37 ± 0.17 (7.25% ± 0.17%)
March	6000 ± 1000	470 ± 66	98 ± 0.074 (1.67% ± 0.074%)	34 ± 0.26 (7.23% ± 0.26%)
April	4200 ± 330	400 ± 61	74 ± 0.081 (1.8% ± 0.081%)	23 ± 0.17 (5.68% ± 0.17%)

317 **Table 1-** Multi-year (2002-2008) Monthly average standard emissions and lead emissions ±1
 318 standard deviation [Gg] and percent change in SSA emissions due to leads ±1 standard deviation
 319 in parentheses (calculated using Eq. (1)) ±1 standard deviation, averaged for 2002-2008, for
 320 ≥60°N and ≥75°N.

321
 322 Table 1 shows the standard and lead emissions in Gg as well as the percent change in multi-year
 323 monthly average SSA emissions due to leads for 60° to 90°N latitude (≥60°N) and 75° to 90°N
 324 (≥75°N). The standard deviations in Table 1 represent the year-to-year variability in emissions, as
 325 the calculation is performed across the 7-year simulation time period for each month. Leads are

Formatted: Justified

Formatted Table

Formatted: Justified

Formatted: Font: 11 pt

Formatted: Font: 11 pt, Font color: Black

Formatted: Justified

Formatted: Font: 11 pt

Formatted: Font: 11 pt

Formatted: Justified

Formatted: Font: 11 pt

Formatted: Font: 11 pt

Formatted: Font: 11 pt

Formatted: Justified

Formatted: Font: 11 pt

Formatted: Font: 11 pt

Formatted: Font: 11 pt

Formatted: Justified

Formatted: Font: 11 pt

Formatted: Font: 11 pt

Formatted: Font: 11 pt

Formatted: Justified

Formatted: Font: 11 pt

Formatted: Font: 11 pt

Formatted: Font: 11 pt

Formatted: Justified

Formatted: Font: 11 pt

Formatted: Font: 11 pt

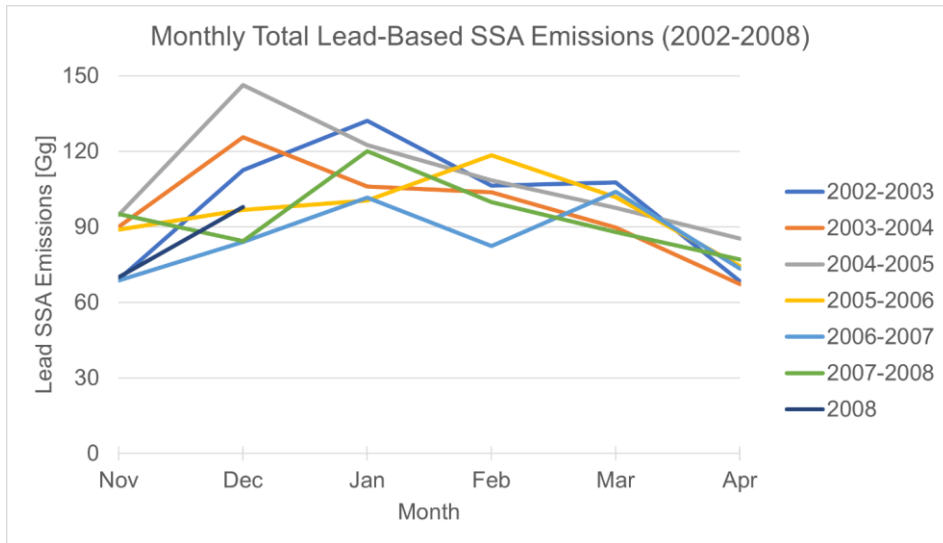
Formatted: Font: Not Bold

Formatted: Justified

326 relatively more important to total SSA emissions at higher latitudes due to large open ocean
 327 emissions in the North Atlantic at lower latitudes (Table 1; see Fig. 2b) and the spatial variability of
 328 the lead emissions (Fig. 2a). The percent increase due to leads is ~4-6% higher for $\geq 75^\circ$ N than
 329 for $\geq 60^\circ$ N latitude. The month with the highest contribution to SSA emissions from leads varies
 330 with the region being analyzed. Poleward of 75° N, SSA emissions increase most from leads in
 331 January, whereas poleward of 60° N, emissions increase most in April. The smaller magnitude of
 332 standard emissions later in the cold season poleward of $\geq 60^\circ$ N make lead emissions relatively
 333 more important than, with the largest percent increase $\geq 60^\circ$ N in SSA emissions due to leads
 334 occurring in April. Poleward of 75° N, the lead emissions represent a larger fraction of the
 335 standard emissions, resulting in higher percent increases due to leads (~4-6% higher than for
 336 $\geq 60^\circ$ N). Absolute lead emissions peak in December for $\geq 75^\circ$ N latitude, which is also the month
 337 with the highest percent increase due to leads $\geq 75^\circ$ N, and decrease more than twofold by April.
 338 Controlling factors of the lead emissions are discussed in the next paragraph. As shown from
 339 the standard deviations in Table 1, there is interannual variability in the percent increases.

340

Formatted: Justified



341

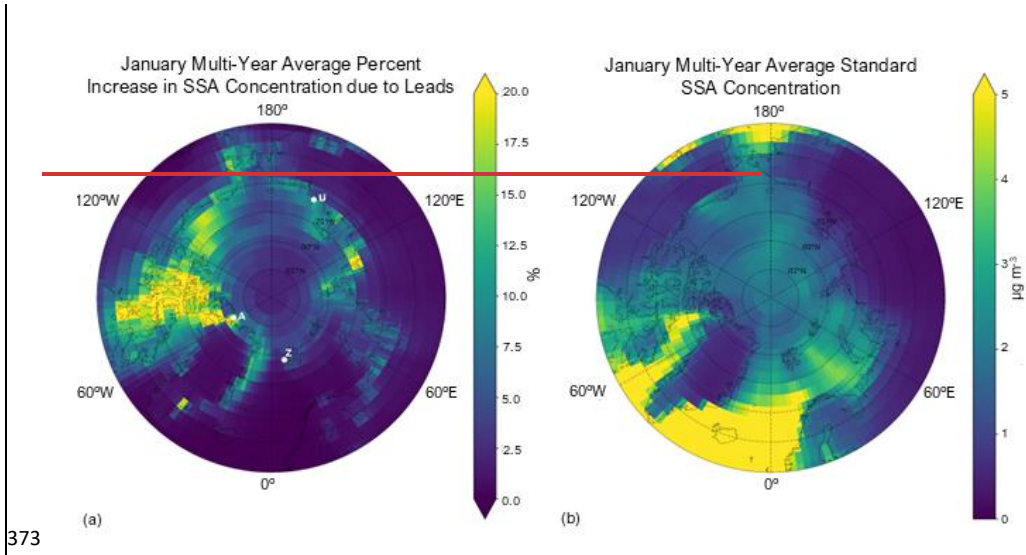
342 **Figure 3-** Monthly variations of total (coarse + accumulation mode) lead emissions of SSA during
 343 the cold season for 2002-2008. Each line includes November and December of the first year and
 344 January through April of the following year, except for the year 2008, which only includes
 345 November and December of 2008.

346
347 We find that the magnitude of lead emissions varies by month and year, as well as seasonally
348 (see Fig. 3 and Figs. S.1 and S.2). Monthly total lead emissions and lead area have low correlation
349 ($R^2 = 0.13$, see Fig. S.3), indicating the variance in monthly total lead emissions is dominated by
350 the nonlinear dependencies on wind speed and sea surface temperature (Eq. S.1 in SI), as the
351 lead emissions are calculated with the Jaegle et al. (2011) wind speed and sea surface
352 temperature source function (see Sect. 2.2). In most years, lead emissions decrease from
353 January-April, but there is no single month when lead emissions peak each year (Fig. 3). There
354 is also no clear interannual trend in cold season total lead emissions (see Fig. S.2). Lead
355 emissions are lowest in the 2006-2007 cold season and highest in the 2004-2005 cold season
356 (Fig. S.2). In the future, climate models predict that Arctic sea ice will continue to thin (high
357 confidence) and the presence of first-year vs. multi-year sea ice will increase (very high
358 confidence) (Intergovernmental Panel On Climate Change, 2023), suggesting a possible future
359 increasing trend in lead area and therefore lead emissions. We find that the annual total lead area
360 in the Arctic over the full period of the AMSR-E satellite data (2002-2011) has statistically
361 significantly increased (see Fig. S.4 (b) and Text S.2 in the SI). Based on satellite observations of
362 leads using methods of detection such as AMSR-2 and thermal infrared satellite imagery, it is
363 unclear if there is a significant observable trend in Arctic lead area from 2011 to the present (Li et
364 al., 2022; Reiser et al., 2020; Wang et al., 2016), especially due to cloud interference with lead
365 detection (Hoffman et al., 2022). However, climate models consistently predict Arctic sea ice will
366 continue to thin (high confidence) and the presence of first year sea ice vs. multi-year sea ice will
367 increase (very high confidence) (Intergovernmental Panel On Climate Change, 2023). This
368 suggests there could be an increasing trend in lead area in the future, which would increase lead
369 emissions.

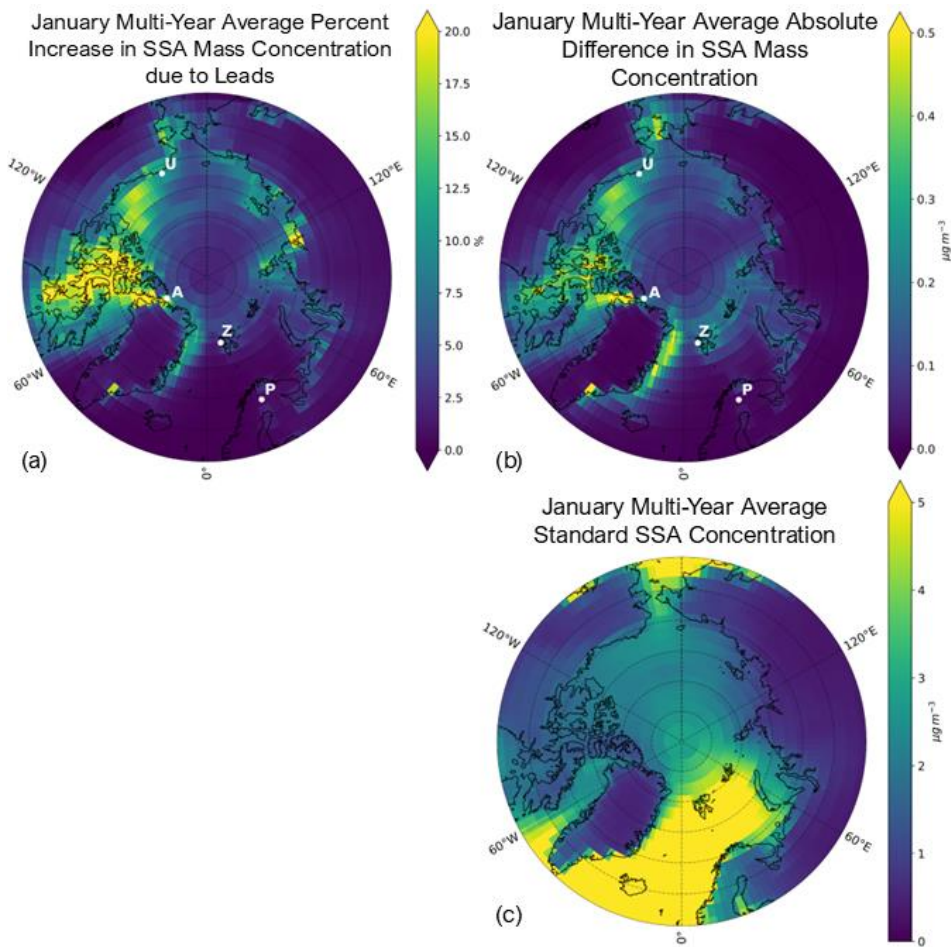
Formatted: Font: (Default) Arial

370 371 3.2 Atmospheric Chemistry Impacts of Sea Ice Leads 372

Formatted: Justified



373



374
 375 **Figure 4-** Percent change due to leads (calculated with Eq. (1)) in SSA mass concentration (a),
 376 absolute difference between the standard+leads and standard SSA mass concentrations in $\mu\text{g m}^{-3}$
 377 (b), and the standard surface SSA mass concentration in $\mu\text{g m}^{-3}$ (c) for the January multi-year
 378 (2002-2008) average. White points in (a) and (b) represent the respective locations of each
 379 observational site: Alert, Nunavut, Canada (A); Utqiagvik, Alaska (U); Zeppelin Mountain,
 380 Svalbard, Norway (Z); Pallas (Matorova), Helsinki, Finland (P). Note the difference in magnitude
 381 of colorbars (b) and (c).

382

Formatted: Centered

Formatted: Justified

383 Figure 4a shows the spatial distribution of the multi-year (2002-2008) average percent change
384 due to leads in surface SSA mass concentration (4a) and the absolute difference in SSA mass
385 concentration between the standard + leads and standard simulations (4b), as well as alongside
386 the standard simulated SSA mass concentration (Fig. 4cb) for the month of January. With the
387 addition of leads, the average Arctic-wide ($\geq 60^\circ\text{N}$) percent increase in multi-year mean January
388 SSA mass concentrations is 3.3%, and the maximum percent increase in an individual model
389 gridbox is 60.5%. We find that the greatest percent increases due to leads in SSA mass
390 concentrations occur at the location of lead emissions (see Fig. 2a), where the standard
391 concentrations are also very low, except off the eastern coast of Greenland, where the percent
392 increase is reduced due to the high background SSA concentrations in the Greenland Sea (Fig.
393 4cb) from open ocean emissions (Fig. 2b).

394
395 Figure 5a shows the average Arctic-wide percent increase and 5c shows the absolute difference
396 due to leads in multi-year monthly mean SSA mass concentration for each cold season month.
397 Averaged poleward of 60°N , the percent increase and absolute difference due to leads in SSA
398 mass concentration remains relatively constant throughout the cold season, ~~but there is a slight~~
399 ~~decreasing trend from November-April when averaged poleward of 75°N~~ (Fig. 5a and c). Changes
400 in monthly mean SSA mass concentrations are also higher poleward of 75°N . However, the
401 percent increase in SSA mass concentration for both latitudinal ranges have large spatial
402 variability, as seen in the standard deviation in Fig. 5a. The spatial distribution of the percent
403 increase and absolute difference in SSA mass concentration due to leads remains similar month
404 to month (see Fig. S.4 and S.5 in SI).

405

Formatted: Justified

Formatted: Justified

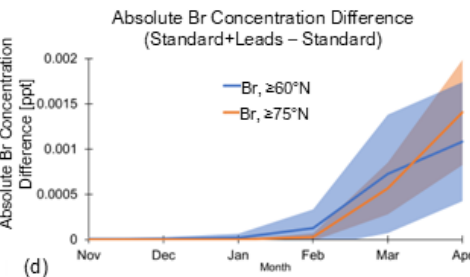
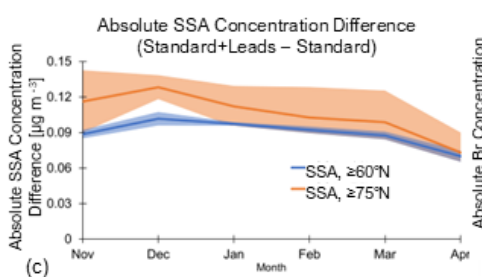
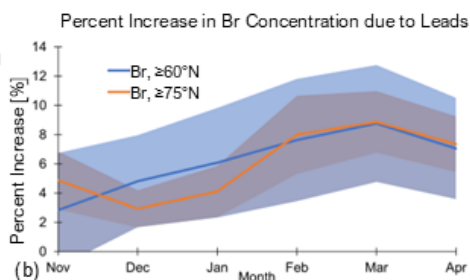
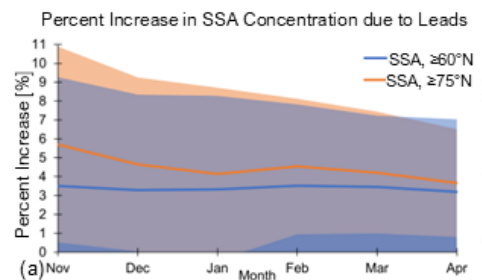
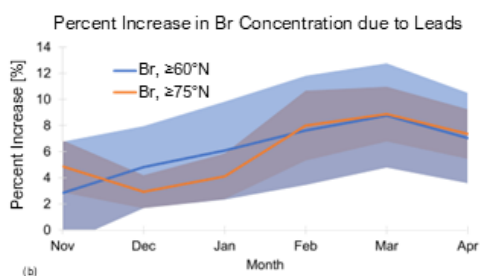
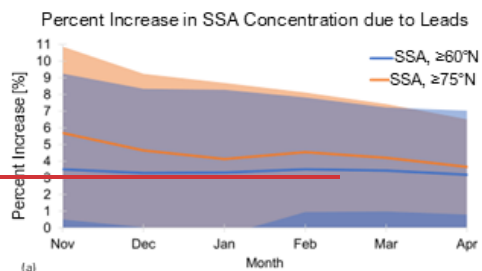
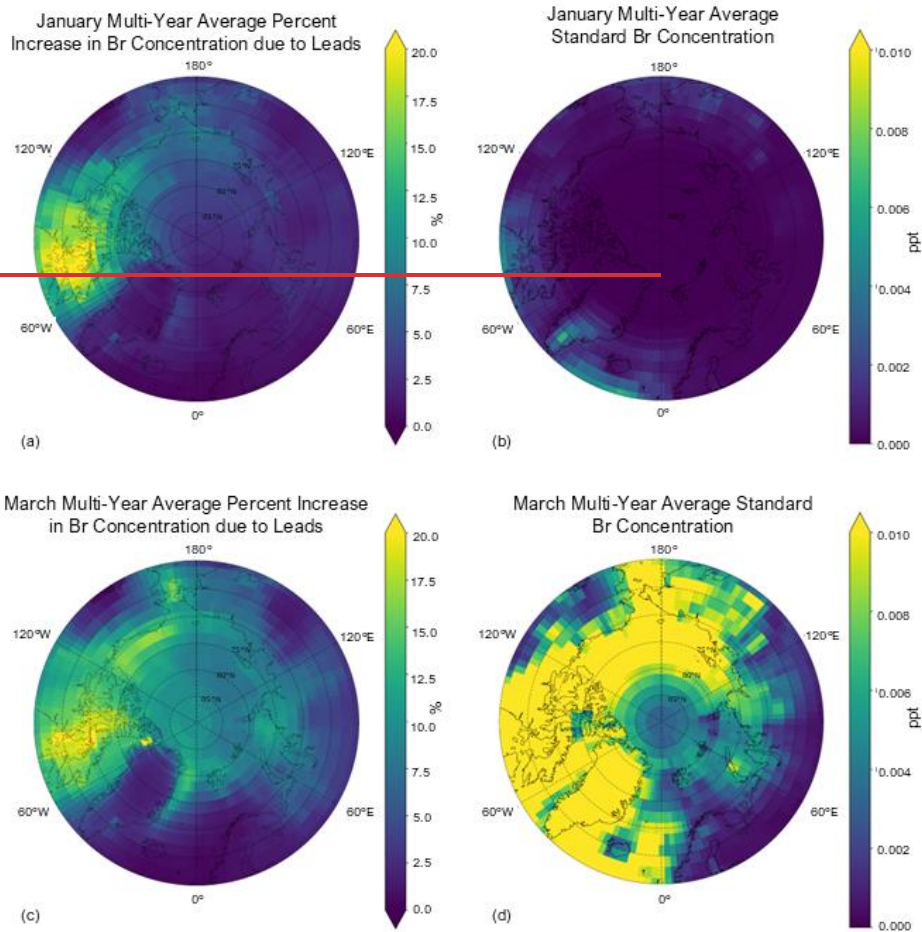


Figure 5. Multi-year (2002-2008) monthly mean percent increase due leads (calculated with Eq. (1)) in surface (a) SSA and (b) Br concentrations averaged across different Arctic regions (blue line: $\geq 60^\circ\text{N}$; orange line: $\geq 75^\circ\text{N}$). Shaded area represents ± 1 standard deviation.

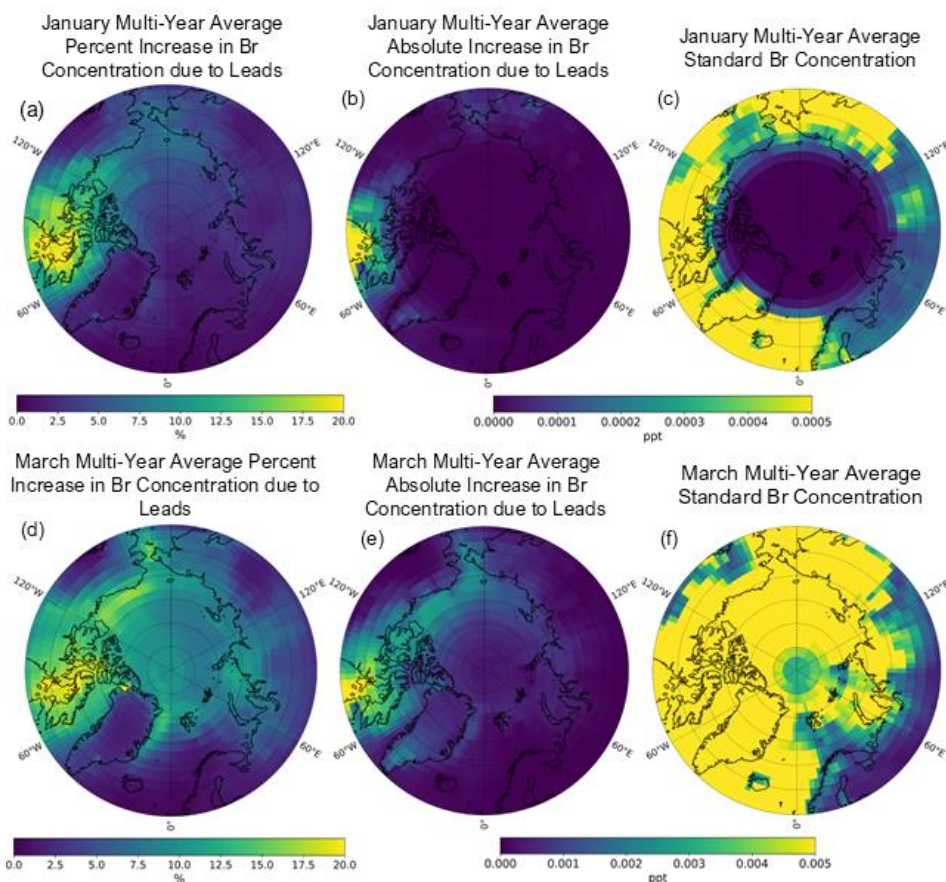
411

412 As described in Sect. 1, SSA contribute to the production of tropospheric reactive bromine and
413 thereby bromine atom (Br). Here we examine changes in Br due to its role in ozone depletion
414 events.

Formatted: Justified



415



Formatted: Centered

416
 417 **Figure 6-** Multi-year (2002-2008) mean January (a, b, and c) and March (d, e, and f) percent increase due to leads in surface Br concentration (a and d), absolute increase in surface
 418 Br concentration due to leads (b and e), and the standard model surface Br concentration in ppt
 419 (c and f). Note the scale of the absolute difference and standard Br concentrations for the
 420 January and March multi-year averages are an order of magnitude difference.
 421

Formatted: Justified

422
 423 Figure 6 shows the multi-year (2002-2008) mean percent increase and absolute difference due
 424 to leads in surface Br concentrations, and the standard Br concentration (in parts per trillion, or
 425 ppt) for the months of January (a-c) and March (d-f), respectively. Increased SSA from leads
 426 increases surface levels of Br across all months during the cold season (Fig. 6a, b, d, and e; Figs.
 427 S.6 and S.7 in the SI for other months). These increased concentrations spatially follow the

428 increased SSA mass concentrations from leads (Fig. 4a; [Figs. S.4 and S.5 in SI for other months](#))
429 with differences due to where Br can be produced photochemically from the precursors released
430 from SSA. The spatial distribution of [the percent increase in Br due to from](#) leads remains
431 relatively similar month to month during the cold season [\(see Fig. S.6 in SI\)](#), but with varying
432 [magnitude \(Fig. 6\)\(see Fig. S.6 in SI\)](#). However, ~~T~~ the changes in Br concentration in February to
433 April occur over a larger area (Fig. 6 ~~d and ee~~ and [Figs. S.6 and S.7](#)), likely due to the seasonality
434 of Arctic bromine chemistry, which is influenced by increasing area where sunlight is available to
435 photolyze Br-sourced SSA species. The average Arctic-wide ($\geq 60^\circ\text{N}$) percent increase due to
436 leads in multi-year January mean surface Br concentration is 6.1% and the maximum increase in
437 an individual gridbox is 35%; for March, it is 8.8% and 20.4%, respectively. Overall, the average
438 monthly percent increase in Br concentration is higher than the corresponding increases in SSA
439 concentration, particularly after January, and reaches a maximum in March (see Fig. 5). The
440 percent change due to leads in Br concentrations increases from November-March poleward of
441 60°N and from December-March poleward of 75°N (Fig. 5b). This does not strictly follow the
442 seasonality of lead emissions (Fig. 3) or the percent increase in SSA concentrations due to leads
443 (Fig. 5a), likely due to more available sunlight for photochemical reactions that produce Br later
444 in the cold season. Increases in surface Br concentration could lead to decreased surface ozone
445 concentrations. We find that the percent decrease due to leads in average surface ozone
446 concentrations during the Arctic cold season, however, are negligible ($< -0.25\%$).

447

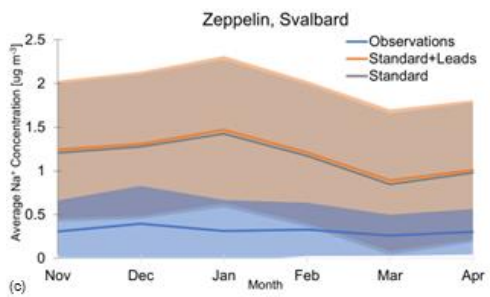
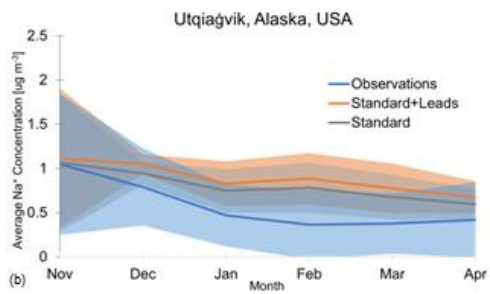
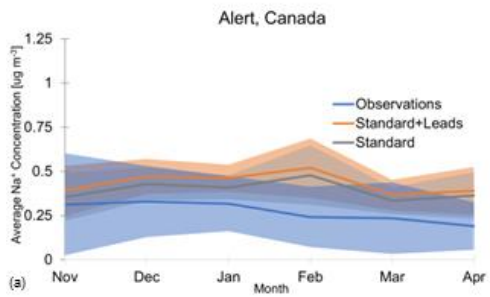
448 3.3 Evaluation Against Sea Salt Aerosol Observations

449

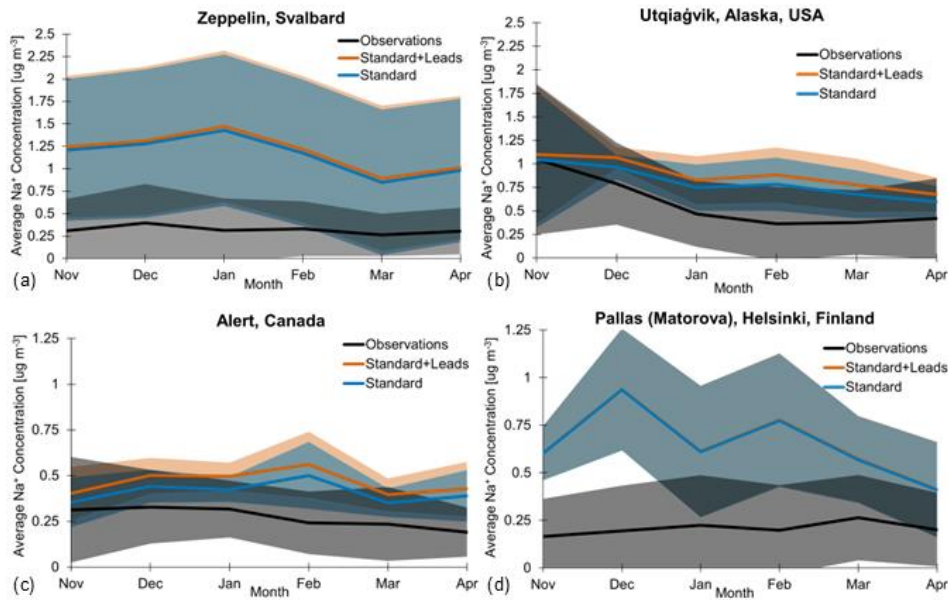
450 We compare modeled and observed sodium (Na^+) mass concentrations at ~~four three~~-long-term
451 monitoring stations to evaluate the performance of the simulation with and without additional lead
452 emissions. The locations of each observational site are shown in Fig. 4a.

453

Formatted: Justified



Formatted: Justified



455
 456 **Figure 7-** Observed (~~blackblue~~ line) and simulated (~~blue gray~~ and orange lines) multi-year
 457 monthly mean sodium mass concentrations at (a) ~~Alert, Canada~~ Zeppelin, Norway, (b) Utqiagvik,
 458 Alaska, ~~and~~ (c) ~~Alert, Canada~~ Zeppelin, Norway, and (d) Pallas (Matorova), Helsinki, Finland
 459 for the cold seasons of 2002-2008 for (a)-(c) and 2003-2008 for (d). Shaded regions are ± 1 standard
 460 deviation. Note the y-axis for Alert (~~ca~~) and Pallas (d) are half as large as Zeppelin (a) and
 461 Utqiagvik (b) and Zeppelin (c).

462
 463 Figure 7 shows multi-year (~~2002-2008~~) monthly mean Na^+ concentrations in the observations
 464 (~~blackblue~~), standard + leads simulation (orange), and standard simulation (~~bluegray~~) for Zeppelin
 465 (a), Utqiagvik (b), Alert (c), and Pallas (d) Alert (7a), Utqiagvik (7b), and Zeppelin (7c) during the
 466 cold season for 2002-2008 (a-c) and 2003-2008 (d). We sample the model simulations in the
 467 gridbox that encompasses the latitude, longitude, and altitude of each monitoring station (see
 468 Sect. 2.3) and convert the simulated SSA to Na^+ concentrations. For all sites and months during
 469 the cold season, the simulated and observed Na^+ mass concentrations overlap within ± 1 standard
 470 deviation (shaded regions in Fig. 7), except in November and December at Pallas. We find mean
 471 concentrations are overpredicted in both the standard and standard + leads simulations at all sites
 472 and months during the cold season, apart from the standard model at Utqiagvik and Alert in
 473 November which agree closest with observations.

Formatted: Justified

474
475 The model overpredicts Na⁺ concentrations the most at Zeppelin and Pallas, with the standard +
476 leads and standard mean concentrations a factor of 3.~~235~~ to 4.71 and 2.0 to 4.8 higher,
477 respectively, than observations across all months during the cold season. Confer et al. (2023)
478 similarly find an overprediction of SSA at Zeppelin, which they find is exacerbated by including
479 blowing snow emissions. Additionally, Zeppelin is at high elevation (located on a mountain at
480 475m) and has been found to be more impacted by the free troposphere and aerosol-cloud
481 interactions than other Arctic sites (Freud et al., 2017); the chemical transport model cannot
482 represent two-way aerosol-cloud interactions. The model overestimate is less at Utqiaġvik, where
483 the standard + leads simulation still overpredicts observed concentrations by a factor of 1.0~~6~~
484 2.4~~3~~, and least at Alert, with observed concentrations overestimated by a factor of 1.~~348~~ to 2.~~345~~
485 for the standard + leads model. Lead emissions do not change the simulated seasonality of cold
486 season surface SSA concentrations. The timing of cold season maximum and minimum
487 concentrations at ~~Alert and Zeppelin~~Zeppelin, Alert, and Pallas differs between the observed and
488 simulated, for both the standard + leads and standard models. At Utqiaġvik, the maximum mass
489 concentration in the observations and both model simulations occurs in November. However, the
490 minimum observed cold season mass concentration occurs in February at Utqiaġvik, whereas the
491 standard + leads and standard mean concentrations reach a minimum in April.

Formatted: Justified

Field Code Changed

Field Code Changed

492
493 Figure 4a and b places the differences seen at each of the three sites in Fig. 7 into broader
494 context, with ~~a-~~maps of the relative and absolute increases in SSA mass concentrations for the
495 month of January. There is minimal change in SSA concentrations where Pallas is located,
496 explaining the near equal Na⁺ concentrations for the standard + leads and standard simulations
497 which results in the overlapping lines in Fig. 7d, suggesting minimal influence from leads at this
498 site. The most significant relative increase in SSA concentration from leads out of the four three
499 sites occurs at Alert (Fig. 7a). However, regions with the highest-largest changes percent
500 increases in SSA mass concentration due to leads in Fig. 4a and b for the month of January (i.e.,
501 parts of Northern Canada southwest of Alert), which are consistent throughout the cold season
502 (Fig. S.4 and S.5 in SI), are not sampled by long-term ground monitoring sites, which would help
503 constrain lead impacts on SSA. In our simulation, lead emissions have the same size distribution
504 as the open ocean, with most of the mass in the coarse mode (82-90%). Despite this, there are
505 increases in SSA concentration over land (Fig. 4a and b) indicating transport (see also Text S.2~~3~~
506 and Fig. S.8~~6~~). This is consistent with observed inland transport of SSA across the North Slope
507 of Alaska (Simpson et al., 2005). It is likely that leads emit smaller SSA particles relative to open

Formatted: Justified

Field Code Changed

508 ocean emissions (Nilsson et al., 2001), which would increase their lifetime, so non-local impacts
509 from leads may be greater than simulated here. This further highlights the need for observations
510 in other regions to better understand the impacts of lead emissions.

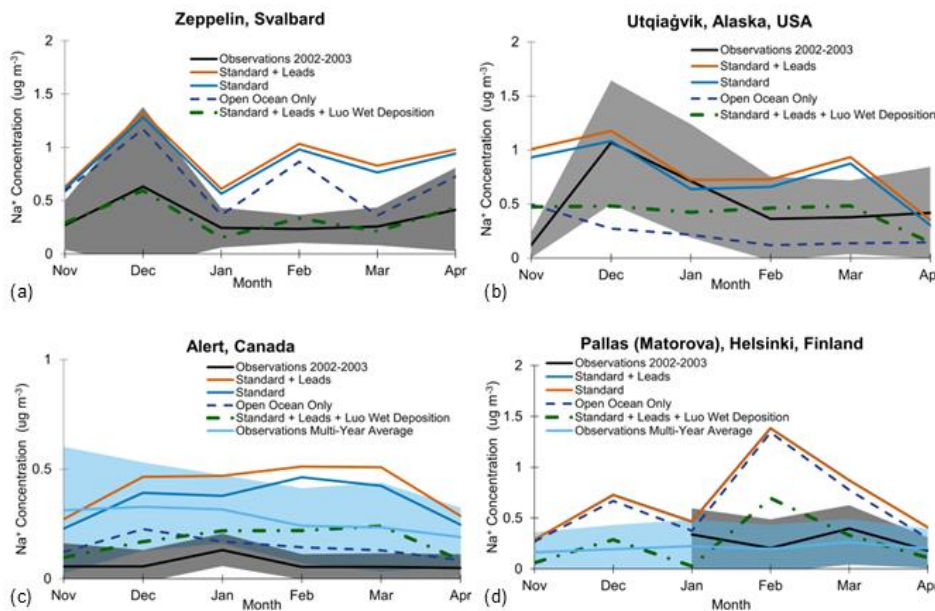
Field Code Changed

511
512 There is strong observational evidence that lead emissions contribute to cold season SSA (see
513 Sect. 1), but the standard model consistently overpredicts observed SSA concentrations prior to
514 inclusion of additional lead emissions. This suggests other sources of SSA may be overpredicted
515 or sinks of SSA may be underpredicted. Ongoing work to improve the treatment of aerosol wet
516 removal processes in GEOS-Chem has not specifically investigated the impacts on sea salt
517 aerosol (Luo et al., 2020; Luo and Yu, 2023). Additionally, a recent observational study (Chen et
518 al., 2022) suggests that the GEOS-Chem blowing snow emissions parameterization may
519 overpredict the frequency of blowing snow events, therefore possibly contributing to the
520 overprediction of Arctic SSA mass concentrations.

Formatted: Justified

Field Code Changed

521



Formatted: Centered

522

523 Figure 8- Model evaluation for the cold season 2002-2003 at Zeppelin (a), Utqiagvik (b), Alert (c),
524 and Pallas (d). Observed Na⁺ concentrations are included as monthly averages for 2002-2003
525 (black + standard deviation margin), and the multi-year monthly averages (light blue + standard
526 deviation margin) (note: no 2002 data is available at Pallas). We show monthly average modeled

527 Na⁺ concentrations for 2002-2003 for the standard + leads (orange) and standard (blue)
528 simulations with two additional sensitivity studies: open ocean only emissions contributing to Na⁺
529 concentrations (dark blue with dashes) and the standard + leads emissions with Luo et al. (2020)
530 wet deposition applied (green line with dashes + dots). Note the different y-axis for Alert (c), as
531 concentrations are much lower at this site.
532

533 To test these possible sources of uncertainty, we run two additional sensitivity simulations for one
534 cold season (November 2002-April 2003): (1) using the Luo et al. (2020) wet deposition scheme
535 with the standard + leads SSA emissions (“standard + leads + Luo Wet Deposition”) and (2)
536 turning off blowing snow emissions in the standard model for an “open ocean only” case (see Text
537 S.4 for further description). We find that the Luo wet deposition scheme improves model
538 agreement most at Zeppelin (see Fig. ~~S-8a(e) in S1~~), especially in the months of November,
539 December, March, and April. At However, at Utqiaġvik, the Luo wet deposition scheme results in
540 underestimates in Na⁺ concentrations compared to observations (Fig. ~~S-8(b)~~ in December,
541 January, and April and overestimates in November, February, and March; however, the
542 overestimated months are closer to the observed concentrations than the standard + leads and
543 standard simulations. Additionally, the standard model at Utqiaġvik agrees with observations in
544 December and the standard + leads model agrees with observations in January and April.
545

546 At Alert, the Luo wet deposition scheme decreases the model overestimate of the standard +
547 leads simulation when compared to the observations for the 2002-2003 cold season (Fig.
548 ~~S-8(ca)~~), but still overestimates Na⁺ concentrations in each month. As the 2002-2003
549 observations at Alert are particularly low, we also include the observed multi-year (2002-2008)
550 monthly average Na⁺ concentrations for comparison. The Luo wet deposition scheme improves
551 model evaluation from February-March compared to the multi-year average observed
552 concentrations at Alert, but otherwise underpredicts concentrations. The Luo wet deposition
553 scheme decreases overprediction at Pallas in February compared to observations from the 2003
554 cold season and improves model agreement in March and April, but underpredicts Na⁺
555 concentrations in January (Fig. 8d). As there are no available observations in 2002 at Pallas, we
556 also include the observed multi-year (2003-2008) monthly average Na⁺ concentrations for
557 comparison. The Luo wet deposition scheme underpredicts Na⁺ concentrations in November,
558 January, and April and overpredicts concentrations in December and March compared to the
559 multi-year average concentrations at Pallas.
560

Formatted: Justified

561 At Utqiagvik, ~~under predicted~~^{too low} Na⁺ concentrations with only open ocean emissions ~~(except~~
562 ~~in November)~~ suggest that this site is influenced by blowing snow emissions and/or lead
563 emissions. Of the ~~four~~^{three} sites, blowing snow is most important and well-represented here, as
564 it also improves the modeled seasonality ~~by correctly representing the December peak in Na⁺~~
565 ~~concentrations in the standard + leads and standard model~~; there may be larger uncertainty in
566 the emissions parameterization in other regions. At Zeppelin ~~and~~, Alert, ~~and~~ Pallas, even with
567 open ocean emissions only and the standard wet deposition, the model overestimates Na⁺
568 concentrations for all months during the cold season for 2002-2003, ~~except at Pallas in January,~~
569 ~~where only open ocean emissions more closely match observations. Moreover, the open ocean~~
570 ~~only Na⁺ concentrations are close in value to the standard + leads and standard concentrations,~~
571 ~~indicating Pallas is largely influenced by open ocean emissions, rather than blowing snow and~~
572 ~~lead emissions.~~

573
574 The results of these sensitivity tests suggest that changes to wet scavenging may be more
575 important at higher altitudes, given the improvement in model evaluation at Zeppelin. Yet, the
576 inclusion of the Luo wet deposition scheme to the standard+leads simulation still overestimates
577 concentrations at Alert, ~~and generally leads to disagreement with observations at Utqiagvik and~~
578 ~~Pallas (except in March and April at Pallas). highlighting there are remaining uncertainties~~
579 ~~associated with the scheme; Luo & Yu (2023) find that it overestimates wet scavenging on a~~
580 ~~global scale. There may be a need for improved representation of the model deposition processes~~
581 ~~to resolve SSA overestimates.~~

583 **4. Uncertainties Discussion**

584
585 ~~Our model evaluation reveals SSA is overestimated in the standard and standard + leads model~~
586 ~~at each of the 4 Arctic sampling sites, pointing to possible sources of uncertainty. First, we use~~
587 ~~the Jaeglé et al. (2011) open ocean function for our lead emissions parameterization as it is the~~
588 ~~standard SSA emission function in GEOS-Chem that has been previously evaluated across global~~
589 ~~oceans. However, there are possible differences in the mechanisms and meteorological~~
590 ~~dependencies of SSA emission from leads vs. the open ocean which could impact the magnitude~~
591 ~~and spatial patterns of lead emissions. Some potential differences were investigated in a~~
592 ~~summertime measurement study (Nilsson et al., 2001), where they derive an empirical lead~~
593 ~~emissions flux equation with an exponential dependence on windspeed and no consideration of~~
594 ~~SST (Eq. (S.2) in SI). They found the emissions rate per area from leads is smaller than that of~~

Formatted: Font: Bold

Formatted: Font: Bold

Formatted: Font: (Default) Arial, 11 pt

Formatted: Font: 11 pt, Font color: Text 1

Formatted: Font: 11 pt, Font color: Text 1

595 the open ocean due to lower fetch in leads, which suggests the lead emissions estimated in our
596 study may be an upper limit when considering large leads only (>3km in size); however, this lead
597 fraction detected by AMSR-E may only include 50% of total lead area (Röhrs and Kaleschke,
598 2012). Additionally, Nilsson et al. (2001) suggest leads emit smaller SSA particles relative to the
599 open ocean, which would increase their lifetime and transport distance. To create a more robust
600 understanding of the different SSA emission mechanisms from leads vs. the open ocean, more
601 studies using size-resolved observations could be conducted within the areas we predict the
602 highest lead emissions, such as within the Bering Strait, Nares Strait, Wynniatt Bay in the
603 Canadian archipelago, and the eastern Greenland Sea.

Formatted: Font: (Default) Arial, 11 pt

Formatted: Font: 11 pt

605 Our sensitivity study results do not ultimately confirm the source(s) of overprediction within the
606 GEOS-Chem model. Blowing snow emissions are included as a standard source of SSA
607 emissions in the Arctic, but remaining uncertainties about the GEOS-Chem blowing snow
608 emissions parameterization (Chen et al., 2022) suggest a need for refinement. Additionally, the
609 results of the standard + leads + Luo wet deposition simulation highlight there are remaining
610 uncertainties associated with wet deposition schemes as the Luo et al. (2020) mechanism does
611 not lead to consistent improvement of simulated SSA concentrations. Luo & Yu (2023) find that
612 the scheme overestimates wet scavenging on a global scale, so continued improvement in the
613 model deposition processes may resolve SSA overestimates.

Formatted: Font: (Default) Arial, 11 pt

Formatted: Font color: Black

614 4.5. Conclusions

617 Observational evidence (Chen et al., 2022; Kirpes et al., 2019; May et al., 2016; Radke et al.,
618 1976; Scott and Levin, 1972; Willis et al., 2018) and one modeling study of the 400 km² region
619 around Utqiagvik, Alaska (Ioannidis et al., 2023)(Ioannidis et al., 2022) have shown that leads
620 may be an important source of cold season SSA for the coastal Arctic. Here, we evaluate their
621 importance as an Arctic-wide source of cold season SSA emissions and their potential
622 atmospheric chemistry impacts in the global chemical transport model GEOS-Chem.

Field Code Changed

Formatted: Font: (Default) Arial, 11 pt

623 We find that lead SSA emissions occur primarily in regions where other SSA emissions sources
624 are very low, mainly within the Bering Strait, Nares Strait, Wynniatt Bay in the Canadian
625 archipelago, and the eastern Greenland Sea. Poleward of 75° N, leads increase total monthly
626 cold-season SSA emissions by 5.68 to 7.58.4%, with the highest contribution of SSA emissions
627 from leads in January and the lowest in April. Lead emissions vary in magnitude by month and
628

Formatted: Justified

629 year, mainly due to variations in lead area. Future trends in Arctic sea ice predicted by climate
630 models suggest a possible future increasing trend in lead area (Intergovernmental Panel On
631 Climate Change, 2023), which would increase lead emissions. ~~Therefore, we expect present day
632 and future lead emissions to be more significant than the time period analyzed in this study (years
633 2002-2008), which could increase atmospheric chemistry impacts.~~ The additional SSA from leads
634 in regions where the background aerosol concentrations are low could also affect local aerosol-
635 cloud interactions, but the overall warming or cooling effect of these additional aerosols remains
636 uncertain (Cox et al., 2015; Schmale et al., 2021; Stramler et al., 2011; Tan et al., 2023; Villanueva
637 et al., 2022). ~~which largely have a warming effect in the Arctic from trapping of longwave radiation
638 during the cold season (Cox et al., 2015; Stramler et al., 2011). This could potentially lead to
639 additional climate feedbacks from expected future climate change driven increases in sea ice lead
640 emissions.~~

Field Code Changed

Formatted: Font: (Default) Arial, 11 pt

Formatted: Justified

642 SSA mass concentrations increase primarily at the location of lead emissions, in regions where
643 the standard SSA mass concentration is very low ($\leq 1.2 \mu\text{g m}^{-3}$). Throughout the cold season, the
644 increased SSA mass concentrations from leads remain relatively constant in magnitude and
645 spatial distribution. The highest increase in multi-year average SSA mass concentrations due to
646 leads, spatially averaged for $\geq 75^\circ\text{N}$, occurs in November ($5.7\% \pm 5.2\%$) and the lowest occurs in
647 April ($3.7\% \pm 2.9\%$). Increased SSA from leads increases surface Br concentrations during the
648 cold season in corresponding locations. ~~The percent increase due to leads in SSA and Br
649 concentrations are spatially coherent.~~ We find total Arctic-wide ($\geq 60^\circ\text{N}$) increases in multi-year
650 mean surface Br concentration range from 2.8 to 8.8%. The increases in Br are not sufficient to
651 have an impact on ozone; subsequent decreases in average surface ozone concentrations in the
652 Arctic are negligible ($< -0.25\%$).

Formatted: Justified

653
654 ~~Our model evaluation reveals SSA is overestimated in the standard and standard+leads model
655 at each of the 3 Arctic sampling sites, which points to possible sources of uncertainty. First,
656 Nilsson et al. (2001) suggest leads emit smaller SSA particles relative to the open ocean, but only
657 Utqiagvik provides aerosol size distinction. There are also no available ground observations
658 where we predict the highest relative increases in SSA mass concentrations. To better constrain
659 lead impacts on SSA and reduce uncertainty in the SSA size distribution, additional ground
660 observations with size distribution information in the Canadian archipelago, such as off the
661 northern coast of Baffin Island and the eastern coast of Victoria Island, would be beneficial. Next,
662 we attempt to better understand the overprediction of SSA mass concentrations with two~~

663 ~~additional sensitivity simulations but are unable to ultimately confirm the source(s) of~~
664 ~~overprediction. Ongoing improvements in the representation of aerosol wet deposition processes~~
665 ~~could significantly impact simulated SSA mass concentrations (Luo et al., 2020; Luo and Yu,~~
666 ~~2023). Additionally, there are uncertainties associated with blowing snow emissions and its~~
667 ~~GEOS-Chem parameterization, suggesting the need for more blowing snow observational~~
668 ~~measurements (such as in the suggested regions for lead emissions measurements) and more~~
669 ~~modeling sensitivity studies. Finally, up to 50% of leads may not be captured in the AMSR-E~~
670 ~~satellite derive lead area product as compared to the MODIS product, while leads covered by thin~~
671 ~~ice, which would not lead to emissions, are included. The net effect of these uncertainties could~~
672 ~~either lead to an underestimate or overestimate of lead SSA emissions in this study. This satellite~~
673 ~~data also covers a past time period (2002-2011), which is not necessarily representative of current~~
674 ~~conditions, so the location and relative importance of lead emissions could have changed.~~

675
676 Overall, we predict sea ice leads may impact Arctic-wide cold-season SSA concentrations and Br
677 concentrations by up to 5-10% on average during the 2002-2008 period. As leads are likely to
678 increase in prevalence under climate change, including this source of SSA in chemistry and
679 climate models ~~may will~~ become more important for future predictions.

680 **Code and Data Availability**

681 Standard model code: <https://doi.org/10.5281/zenodo.5500717>; AMSR-E data:
682 <https://www.cen.uni-hamburg.de/en/icdc/data/cryosphere/lead-area-fraction-amsre.html>;
683 observational site data (Alert, Pallas, and Zeppelin): <https://ebas-data.nilu.no/Default.aspx>;
684 observational data (Utqiaġvik): <https://saga.pmel.noaa.gov/data/stations/>;
685 model data shown in
686 paper: <https://doi.org/10.5281/zenodo.14611355>.

687 **Author Contribution**

688 EJE was responsible for data curation, model simulations, validation, visualization, and analysis
689 with expert advice from HMM. HMM is responsible for conceptualization. EJE drafted the
690 manuscript which was revised by HMM.
691

692 **Competing Interests**

693 The authors declare that they have no conflict of interest.

694 **Acknowledgements**

Formatted: Justified

Formatted: Font: Not Bold

Formatted: Font: Not Bold

Formatted: Justified

697 We thank Kerri Pratt for helpful discussions. HMH was supported by Department of Energy (DOE)
698 Atmospheric Systems Research (ASR), award DE-SC0023049. We acknowledge financial
699 support from the department of Civil and Environmental Engineering at the University of Illinois
700 Urbana-Champaign.

701

Formatted: Justified

702 Supplemental Information

703 Equations of SSA flux from Jaegle et al. (2011) and Nilsson et al. (2001); Additional figures of lead
704 SSA emissions for months other than January during the cold season; Cold season total lead
705 SSA emissions; Description and figure of the correlation between lead area and lead SSA
706 emissions; long-term trends in lead area (2002-2011) and relevant statistical testing; additional
707 figures of multi-year (2002-2008) mean percent increase due to leads in SSA and bromine
708 concentration for months other than January during the cold season; Description and figures of
709 correlation between lead emissions and coarse and accumulation mode SSA concentration;
710 Sensitivity simulations.

711

Formatted: Justified

712 5-6. References

713

Field Code Changed

714 [Abbatt, J. P. D., Thomas, J. L., Abrahamsson, K., Boxe, C., Granfors, A., Jones, A. E., King, M. D., Saiz-
715 Lopez, A., Shepson, P. B., Sodeau, J., Toohey, D. W., Toubin, C., Von Glasow, R., Wren, S. N., and Yang,
716 X.: Halogen activation via interactions with environmental ice and snow in the polar lower troposphere
717 and other regions, *Atmospheric Chem. Phys.*, 12, 6237–6271, <https://doi.org/10.5194/acp-12-6237-2012>,
718 2012.](#)

719 [Alvarez-Aviles, L., Simpson, W. R., Douglas, T. A., Sturm, M., Perovich, D., and Domine, F.: Frost
720 flower chemical composition during growth and its implications for aerosol production and bromine
721 activation, *J. Geophys. Res. Atmospheres*, 113, 2008JD010277, <https://doi.org/10.1029/2008JD010277>,
722 2008.](#)

723 [Amos, H. M., Jacob, D. J., Holmes, C. D., Fisher, J. A., Wang, Q., Yantosca, R. M., Corbitt, E. S.,
724 Galarrneau, E., Rutter, A. P., Gustin, M. S., Steffen, A., Schauer, J. J., Graydon, J. A., Louis, V. L. St.,
725 Talbot, R. W., Edgerton, E. S., Zhang, Y., and Sunderland, E. M.: Gas-particle partitioning of atmospheric
726 Hg\(II\) and its effect on global mercury deposition, *Atmospheric Chem. Phys.*, 12, 591–603,
727 <https://doi.org/10.5194/acp-12-591-2012>, 2012.](#)

728 [Chen, Q., Mirrielees, J. A., Thanekar, S., Loeb, N. A., Kirpes, R. M., Upchurch, L. M., Barget, A. J., Lata,
729 N. N., Raso, A. R. W., McNamara, S. M., China, S., Quinn, P. K., Ault, A. P., Kennedy, A., Shepson, P. B.,
730 Fuentes, J. D., and Pratt, K. A.: Atmospheric particle abundance and sea salt aerosol observations in the
731 springtime Arctic: a focus on blowing snow and leads, *Atmospheric Chem. Phys.*, 22, 15263–15285,
732 <https://doi.org/10.5194/acp-22-15263-2022>, 2022.](#)

733 [Confer, K. L., Jaeglé, L., Liston, G. E., Sharma, S., Nandan, V., Yackel, J., Ewert, M., and Horowitz, H.
734 M.: Impact of Changing Arctic Sea Ice Extent, Sea Ice Age, and Snow Depth on Sea Salt Aerosol From](#)

735 [Blowing Snow and the Open Ocean for 1980–2017, J. Geophys. Res. Atmospheres, 128, e2022JD037667,](https://doi.org/10.1029/2022JD037667)
736 [https://doi.org/10.1029/2022JD037667, 2023.](https://doi.org/10.1029/2022JD037667)

737 [Cox, C. J., Walden, V. P., Rowe, P. M., and Shupe, M. D.: Humidity trends imply increased sensitivity to](https://doi.org/10.1038/ncomms10117)
738 [clouds in a warming Arctic, Nat. Commun., 6, 10117, https://doi.org/10.1038/ncomms10117, 2015.](https://doi.org/10.1038/ncomms10117)

739 [DeMott, P. J., Hill, T. C. J., McCluskey, C. S., Prather, K. A., Collins, D. B., Sullivan, R. C., Ruppel, M.](https://doi.org/10.1073/pnas.1514034112)
740 [J., Mason, R. H., Irish, V. E., Lee, T., Hwang, C. Y., Rhee, T. S., Snider, J. R., McMeeking, G. R.,](https://doi.org/10.1073/pnas.1514034112)
741 [Dhaniyala, S., Lewis, E. R., Wentzell, J. J. B., Abbatt, J., Lee, C., Sultana, C. M., Ault, A. P., Axson, J. L.,](https://doi.org/10.1073/pnas.1514034112)
742 [Diaz Martinez, M., Venero, I., Santos-Figueroa, G., Stokes, M. D., Deane, G. B., Mayol-Bracero, O. L.,](https://doi.org/10.1073/pnas.1514034112)
743 [Grassian, V. H., Bertram, T. H., Bertram, A. K., Moffett, B. F., and Franc, G. D.: Sea spray aerosol as a](https://doi.org/10.1073/pnas.1514034112)
744 [unique source of ice nucleating particles, Proc. Natl. Acad. Sci., 113, 5797–5803,](https://doi.org/10.1073/pnas.1514034112)
745 [https://doi.org/10.1073/pnas.1514034112, 2016.](https://doi.org/10.1073/pnas.1514034112)

746 [Dibb, J. E., Ziemba, L. D., Luxford, J., and Beckman, P.: Bromide and other ions in the snow, firn air, and](https://doi.org/10.5194/acp-10-9931-2010)
747 [atmospheric boundary layer at Summit during GSHOX, Atmospheric Chem. Phys., 10, 9931–9942,](https://doi.org/10.5194/acp-10-9931-2010)
748 [https://doi.org/10.5194/acp-10-9931-2010, 2010.](https://doi.org/10.5194/acp-10-9931-2010)

749 [Domine, F., Sparapani, R., Ianniello, A., and Beine, H. J.: The origin of sea salt in snow on Arctic sea ice](https://doi.org/10.5194/acp-4-2259-2004)
750 [and in coastal regions, Atmospheric Chem. Phys., 4, 2259–2271, https://doi.org/10.5194/acp-4-2259-](https://doi.org/10.5194/acp-4-2259-2004)
751 [2004, 2004.](https://doi.org/10.5194/acp-4-2259-2004)

752 [Freud, E., Krejci, R., Tunved, P., Leaitch, R., Nguyen, Q. T., Massling, A., Skov, H., and Barrie, L.: Pan-](https://doi.org/10.5194/acp-17-8101-2017)
753 [Arctic aerosol number size distributions: seasonality and transport patterns, Atmospheric Chem. Phys.,](https://doi.org/10.5194/acp-17-8101-2017)
754 [17, 8101–8128, https://doi.org/10.5194/acp-17-8101-2017, 2017.](https://doi.org/10.5194/acp-17-8101-2017)

755 [Gelaro, R., McCarty, W., Suárez, M. J., Todling, R., Molod, A., Takacs, L., Randles, C. A., Darmenov, A.,](https://doi.org/10.1175/JCLI-D-16-0758.1)
756 [Bosilovich, M. G., Reichle, R., Wargan, K., Coy, L., Cullather, R., Draper, C., Akella, S., Buchard, V.,](https://doi.org/10.1175/JCLI-D-16-0758.1)
757 [Conaty, A., Da Silva, A. M., Gu, W., Kim, G.-K., Koster, R., Lucchesi, R., Merkova, D., Nielsen, J. E.,](https://doi.org/10.1175/JCLI-D-16-0758.1)
758 [Partyka, G., Pawson, S., Putman, W., Rienecker, M., Schubert, S. D., Sienkiewicz, M., and Zhao, B.: The](https://doi.org/10.1175/JCLI-D-16-0758.1)
759 [Modern-Era Retrospective Analysis for Research and Applications, Version 2 \(MERRA-2\), J. Clim., 30,](https://doi.org/10.1175/JCLI-D-16-0758.1)
760 [5419–5454, https://doi.org/10.1175/JCLI-D-16-0758.1, 2017.](https://doi.org/10.1175/JCLI-D-16-0758.1)

761 [Gong, S. L.: A parameterization of sea-salt aerosol source function for sub- and super-micron particles,](https://doi.org/10.1029/2003GB002079)
762 [Glob. Biogeochem. Cycles, 17, 2003GB002079, https://doi.org/10.1029/2003GB002079, 2003.](https://doi.org/10.1029/2003GB002079)

763 [Held, A., Brooks, I. M., Leck, C., and Tjernström, M.: On the potential contribution of open lead particle](https://doi.org/10.5194/acp-11-3093-2011)
764 [emissions to the central Arctic aerosol concentration, Atmospheric Chem. Phys., 11, 3093–3105,](https://doi.org/10.5194/acp-11-3093-2011)
765 [https://doi.org/10.5194/acp-11-3093-2011, 2011.](https://doi.org/10.5194/acp-11-3093-2011)

766 [Huang, J. and Jaeglé, L.: Wintertime enhancements of sea salt aerosol in polar regions consistent with a](https://doi.org/10.5194/acp-17-3699-2017)
767 [sea ice source from blowing snow, Atmospheric Chem. Phys., 17, 3699–3712,](https://doi.org/10.5194/acp-17-3699-2017)
768 [https://doi.org/10.5194/acp-17-3699-2017, 2017.](https://doi.org/10.5194/acp-17-3699-2017)

769 [Huang, J., Jaeglé, L., and Shah, V.: Using CALIOP to constrain blowing snow emissions of sea salt](https://doi.org/10.5194/acp-18-16253-2018)
770 [aerosols over Arctic and Antarctic sea ice, Atmospheric Chem. Phys., 18, 16253–16269,](https://doi.org/10.5194/acp-18-16253-2018)
771 [https://doi.org/10.5194/acp-18-16253-2018, 2018.](https://doi.org/10.5194/acp-18-16253-2018)

772 [Huang, J., Jaeglé, L., Chen, Q., Alexander, B., Sherwen, T., Evans, M. J., Theys, N., and Choi, S.:](https://doi.org/10.5194/acp-18-16253-2018)
773 [Evaluating the impact of blowing-snow sea salt aerosol on springtime BrO and](https://doi.org/10.5194/acp-18-16253-2018)

774 [O<sub>3</sub> in the Arctic. Atmospheric Chem. Phys., 20, 7335–7358,](#)
775 <https://doi.org/10.5194/acp-20-7335-2020>, 2020.

776 [Integrated Climate Data Center \(ICDC\), CEN, and University of Hamburg, Hamburg, Germany: AMSR-](#)
777 [E Arctic lead area fraction, n.d.](#)

778 [Intergovernmental Panel On Climate Change: Climate Change 2021 – The Physical Science Basis:](#)
779 [Working Group I Contribution to the Sixth Assessment Report of the Intergovernmental Panel on Climate](#)
780 [Change, 1st ed., Cambridge University Press, https://doi.org/10.1017/9781009157896, 2023.](#)

781 [Ioannidis, E., Law, K. S., Raut, J.-C., Marelle, L., Onishi, T., Kirpes, R. M., Upchurch, L. M., Tuch, T.,](#)
782 [Wiedensohler, A., Massling, A., Skov, H., Quinn, P. K., and Pratt, K. A.: Modelling wintertime sea-spray](#)
783 [aerosols under Arctic haze conditions, Atmospheric Chem. Phys., 23, 5641–5678,](#)
784 <https://doi.org/10.5194/acp-23-5641-2023>, 2023.

785 [Jaeglé, L., Quinn, P. K., Bates, T. S., Alexander, B., and Lin, J.-T.: Global distribution of sea salt aerosols:](#)
786 [new constraints from in situ and remote sensing observations, Atmospheric Chem. Phys., 11, 3137–3157,](#)
787 <https://doi.org/10.5194/acp-11-3137-2011>, 2011.

788 [Keller, C. A., Long, M. S., Yantosca, R. M., Da Silva, A. M., Pawson, S., and Jacob, D. J.: HEMCO v1.0:](#)
789 [a versatile, ESMF-compliant component for calculating emissions in atmospheric models, Geosci. Model](#)
790 [Dev., 7, 1409–1417, https://doi.org/10.5194/gmd-7-1409-2014, 2014.](#)

791 [Kirpes, R. M., Bonanno, D., May, N. W., Fraund, M., Barget, A. J., Moffet, R. C., Ault, A. P., and Pratt, K.](#)
792 [A.: Wintertime Arctic Sea Spray Aerosol Composition Controlled by Sea Ice Lead Microbiology, ACS](#)
793 [Cent. Sci., 5, 1760–1767, https://doi.org/10.1021/acscentsci.9b00541, 2019.](#)

794 [Leaitch, W. R., Russell, L. M., Liu, J., Kolonjari, F., Toom, D., Huang, L., Sharma, S., Chivulescu, A.,](#)
795 [Veber, D., and Zhang, W.: Organic functional groups in the submicron aerosol at 82.5° N, 62.5° W from](#)
796 [2012 to 2014, Atmospheric Chem. Phys., 18, 3269–3287, https://doi.org/10.5194/acp-18-3269-2018,](#)
797 [2018.](#)

798 [Lin, H., Jacob, D. J., Lundgren, E. W., Sulprizio, M. P., Keller, C. A., Fritz, T. M., Eastham, S. D.,](#)
799 [Emmons, L. K., Campbell, P. C., Baker, B., Saylor, R. D., and Montuoro, R.: Harmonized Emissions](#)
800 [Component \(HEMCO\) 3.0 as a versatile emissions component for atmospheric models: application in the](#)
801 [GEOS-Chem, NASA GEOS, WRF-GC, CESM2, NOAA GEFS-Aerosol, and NOAA UFS models,](#)
802 [Geosci. Model Dev., 14, 5487–5506, https://doi.org/10.5194/gmd-14-5487-2021, 2021.](#)

803 [Liu, H., Jacob, D. J., Bey, I., and Yantosca, R. M.: Constraints from ²¹⁰Pb and ⁷Be on wet deposition and](#)
804 [transport in a global three-dimensional chemical tracer model driven by assimilated meteorological fields,](#)
805 [J. Geophys. Res. Atmospheres, 106, 12109–12128, https://doi.org/10.1029/2000JD900839, 2001.](#)

806 [Luo, G. and Yu, F.: Impact of Air Refreshing and Cloud Ice Uptake Limitations on Vertical Profiles and](#)
807 [Wet Depositions of Nitrate, Ammonium, and Sulfate, Geophys. Res. Lett., 50, e2023GL104258,](#)
808 <https://doi.org/10.1029/2023GL104258>, 2023.

809 [Luo, G., Yu, F., and Moch, J. M.: Further improvement of wet process treatments in GEOS-Chem](#)
810 [v12.6.0: impact on global distributions of aerosols and aerosol precursors, Geosci. Model Dev., 13, 2879–](#)
811 [2903, https://doi.org/10.5194/gmd-13-2879-2020, 2020.](#)

812 [May, N. W., Quinn, P. K., McNamara, S. M., and Pratt, K. A.: Multiyear study of the dependence of sea](#)
813 [salt aerosol on wind speed and sea ice conditions in the coastal Arctic, J. Geophys. Res. Atmospheres,](#)
814 [121, 9208–9219, <https://doi.org/10.1002/2016JD025273>, 2016.](#)

815 [Monahan, E. C., Spiel, D. E., and Davidson, K. L.: A Model of Marine Aerosol Generation Via Whitecaps](#)
816 [and Wave Disruption, in: Oceanic Whitecaps, vol. 2, edited by: Monahan, E. C. and Niocaill, G. M.,](#)
817 [Springer Netherlands, Dordrecht, 167–174, \[https://doi.org/10.1007/978-94-009-4668-2_16\]\(https://doi.org/10.1007/978-94-009-4668-2_16\), 1986.](#)

818 [Nilsson, E. D., Rannik, Ü., Swietlicki, E., Leck, C., Aalto, P. P., Zhou, J., and Norman, M.: Turbulent](#)
819 [aerosol fluxes over the Arctic Ocean: 2. Wind-driven sources from the sea, J. Geophys. Res. Atmospheres,](#)
820 [106, 32139–32154, <https://doi.org/10.1029/2000JD900747>, 2001.](#)

821 [Pierce, J. R. and Adams, P. J.: Global evaluation of CCN formation by direct emission of sea salt and](#)
822 [growth of ultrafine sea salt, J. Geophys. Res. Atmospheres, 111, 2005JD006186,](#)
823 [https://doi.org/10.1029/2005JD006186, 2006.](#)

824 [Pound, R. J., Sherwen, T., Helmig, D., Carpenter, L. J., and Evans, M. J.: Influences of oceanic ozone](#)
825 [deposition on tropospheric photochemistry, Atmospheric Chem. Phys., 20, 4227–4239,](#)
826 [https://doi.org/10.5194/acp-20-4227-2020, 2020.](#)

827 [Pratt, K. A., Custard, K. D., Shepson, P. B., Douglas, T. A., Pöhler, D., General, S., Zielcke, J., Simpson,](#)
828 [W. R., Platt, U., Tanner, D. J., Gregory Huey, L., Carlsen, M., and Stirm, B. H.: Photochemical production](#)
829 [of molecular bromine in Arctic surface snowpacks, Nat. Geosci., 6, 351–356,](#)
830 [https://doi.org/10.1038/ngeo1779, 2013.](#)

831 [Quinn, P. K., Coffman, D. J., Kapustin, V. N., Bates, T. S., and Covert, D. S.: Aerosol optical properties in](#)
832 [the marine boundary layer during the First Aerosol Characterization Experiment \(ACE 1\) and the](#)
833 [underlying chemical and physical aerosol properties, J. Geophys. Res., 103, 16,547–16,563, 1998.](#)

834 [Quinn, P. K., Bates, T. S., Miller, T. L., Coffman, D. J., Johnson, J. E., Harris, J. M., Ogren, J. A., Forbes,](#)
835 [G., Anderson, T. L., Covert, D. S., and Rood, M. J.: Surface submicron aerosol chemical composition:](#)
836 [What fraction is not sulfate?, J. Geophys. Res. Atmospheres, 105, 6785–6805,](#)
837 [https://doi.org/10.1029/1999JD901034, 2000.](#)

838 [Quinn, P. K., Miller, T. L., Bates, T. S., Ogren, J. A., Andrews, E., and Shaw, G. E.: A 3-year record of](#)
839 [simultaneously measured aerosol chemical and optical properties at Barrow, Alaska, J. Geophys. Res.](#)
840 [Atmospheres, 107, <https://doi.org/10.1029/2001JD001248>, 2002.](#)

841 [Radke, L. F., Hobbs, P. V., and Pinnons, J. E.: Observations of Cloud Condensation Nuclei, Sodium-](#)
842 [Containing Particles, Ice Nuclei and the Light-Scattering Coefficient Near Barrow, Alaska, J. Appl.](#)
843 [Meteor. Climatol., 15, 982–995, <https://doi.org/10.1175/1520->](#)
844 [0450\(1976\)015%3C0982:OOCNS%3E2.0.CO;2, 1976.](#)

845 [Rhodes, R. H., Yang, X., Wolff, E. W., McConnell, J. R., and Frey, M. M.: Sea ice as a source of sea salt](#)
846 [aerosol to Greenland ice cores: a model-based study, Atmospheric Chem. Phys., 17, 9417–9433,](#)
847 [https://doi.org/10.5194/acp-17-9417-2017, 2017.](#)

848 [Riley, J. P. and Chester, R.: Introduction to marine chemistry, Academic Press, London, New York, 465](#)
849 [pp., 1971.](#)

850 [Röhrs, J. and Kaleschke, L.: An algorithm to detect sea ice leads by using AMSR-E passive microwave](#)
851 [imagery, *The Cryosphere*, 6, 343–352, <https://doi.org/10.5194/tc-6-343-2012>, 2012.](#)

852 [Roscoe, H. K., Brooks, B., Jackson, A. V., Smith, M. H., Walker, S. J., Obbard, R. W., and Wolff, E. W.:](#)
853 [Frost flowers in the laboratory: Growth, characteristics, aerosol, and the underlying sea ice, *J. Geophys.*](#)
854 [Res., 116, D12301, <https://doi.org/10.1029/2010JD015144>, 2011.](#)

855 [Salmi, T.: Measurement of Inorganics in air and particle phase at Pallas \(Matorova\) \(3\),](#)
856 [<https://doi.org/10.48597/T6MX-CEKH>, 2018.](#)

857 [Schmale, J., Zieger, P., and Ekman, A. M. L.: Aerosols in current and future Arctic climate, *Nat. Clim.*](#)
858 [Change, 11, 95–105, <https://doi.org/10.1038/s41558-020-00969-5>, 2021.](#)

859 [Scott, W. D. and Levin, Z.: Open Channels in Sea Ice \(Leads\) as Ion Sources, *Science*, 177, 425–426,](#)
860 [<https://doi.org/10.1126/science.177.4047.425>, 1972.](#)

861 [Screen, J. A. and Simmonds, I.: Declining summer snowfall in the Arctic: causes, impacts and feedbacks,](#)
862 [*Clim. Dyn.*, 38, 2243–2256, <https://doi.org/10.1007/s00382-011-1105-2>, 2012.](#)

863 [Simpson, W. R., Alvarez-Aviles, L., Douglas, T. A., Sturm, M., and Domine, F.: Halogens in the coastal](#)
864 [snow pack near Barrow, Alaska: Evidence for active bromine air-snow chemistry during springtime,](#)
865 [*Geophys. Res. Lett.*, 32, 2004GL021748, <https://doi.org/10.1029/2004GL021748>, 2005.](#)

866 [Simpson, W. R., Von Glasow, R., Riedel, K., Anderson, P., Ariya, P., Bottenheim, J., Burrows, J.,](#)
867 [Carpenter, L. J., Frieß, U., Goodsite, M. E., Heard, D., Hutterli, M., Jacobi, H.-W., Kaleschke, L., Neff,](#)
868 [B., Plane, J., Platt, U., Richter, A., Roscoe, H., Sander, R., Shepson, P., Sodeau, J., Steffen, A., Wagner, T.,](#)
869 [and Wolff, E.: Halogens and their role in polar boundary-layer ozone depletion, *Atmospheric Chem.*](#)
870 [Phys., 7, 4375–4418, <https://doi.org/10.5194/acp-7-4375-2007>, 2007.](#)

871 [Stramler, K., Del Genio, A. D., and Rossow, W. B.: Synoptically Driven Arctic Winter States, *J. Clim.*, 24,](#)
872 [1747–1762, <https://doi.org/10.1175/2010JCLI3817.1>, 2011.](#)

873 [Stutz, J., Thomas, J. L., Hurlock, S. C., Schneider, M., Von Glasow, R., Piot, M., Gorham, K., Burkhart, J.](#)
874 [F., Ziemba, L., Dibb, J. E., and Lefer, B. L.: Longpath DOAS observations of surface BrO at Summit,](#)
875 [Greenland, *Atmospheric Chem. Phys.*, 11, 9899–9910, <https://doi.org/10.5194/acp-11-9899-2011>, 2011.](#)

876 [Sumata, H., De Steur, L., Divine, D. V., Granskog, M. A., and Gerland, S.: Regime shift in Arctic Ocean](#)
877 [sea ice thickness, *Nature*, 615, 443–449, <https://doi.org/10.1038/s41586-022-05686-x>, 2023.](#)

878 [Swanson, W. F., Holmes, C. D., Simpson, W. R., Confer, K., Marelle, L., Thomas, J. L., Jaeglé, L.,](#)
879 [Alexander, B., Zhai, S., Chen, Q., Wang, X., and Sherwen, T.: Comparison of model and ground](#)
880 [observations finds snowpack and blowing snow aerosols both contribute to Arctic tropospheric reactive](#)
881 [bromine, *Atmospheric Chem. Phys.*, 22, 14467–14488, <https://doi.org/10.5194/acp-22-14467-2022>, 2022.](#)

882 [Tan, I., Sotiropoulou, G., Taylor, P. C., Zamora, L., and Wendisch, M.: A Review of the Factors](#)
883 [Influencing Arctic Mixed-Phase Clouds: Progress and Outlook, in: *Geophysical Monograph Series*, edited](#)
884 [by: Sullivan, S. C. and Hoose, C., Wiley, 103–132, <https://doi.org/10.1002/9781119700357.ch5>, 2023.](#)

885 [Vaughan, D., Comiso, J., Allison, I., Carrasco, J., Kaser, G., Kwok, R., Mote, P., Murray, T., Paul, F., Ren,](#)
886 [J. F., Rignot, E., Solomina, O., Steffen, K., and Zhang, T.: Observations: Cryosphere, in: *Climate Change*](#)
887 [2013: The Physical Science Basis, 317–382, 2013.](#)

888 [Villanueva, D., Possner, A., Neubauer, D., Gasparini, B., Lohmann, U., and Tesche, M.: Mixed-phase](#)
889 [regime cloud thinning could help restore sea ice, *Environ. Res. Lett.*, 17, 114057,](#)
890 <https://doi.org/10.1088/1748-9326/aca16d>, 2022.

891 [Wang, Q., Jacob, D. J., Spackman, J. R., Perring, A. E., Schwarz, J. P., Moteki, N., Marais, E. A., Ge, C.,](#)
892 [Wang, J., and Barrett, S. R. H.: Global budget and radiative forcing of black carbon aerosol: Constraints](#)
893 [from pole-to-pole \(HIPPO\) observations across the Pacific, *J. Geophys. Res. Atmospheres*, 119, 195–206,](#)
894 <https://doi.org/10.1002/2013JD020824>, 2014.

895 [Wang, X., Jacob, D. J., Downs, W., Zhai, S., Zhu, L., Shah, V., Holmes, C. D., Sherwen, T., Alexander, B.,](#)
896 [Evans, M. J., Eastham, S. D., Neuman, J. A., Veres, P. R., Koenig, T. K., Volkamer, R., Huey, L. G.,](#)
897 [Bannan, T. J., Percival, C. J., Lee, B. H., and Thornton, J. A.: Global tropospheric halogen \(Cl, Br, I\)](#)
898 [chemistry and its impact on oxidants, *Atmospheric Chem. Phys.*, 21, 13973–13996,](#)
899 <https://doi.org/10.5194/acp-21-13973-2021>, 2021.

900 [Wang, Y., Jacob, D. J., and Logan, J. A.: Global simulation of tropospheric O₃-NO_x-hydrocarbon](#)
901 [chemistry: 3. Origin of tropospheric ozone and effects of nonmethane hydrocarbons, *J. Geophys. Res.*](#)
902 [Atmospheres, 103, 10757–10767, <https://doi.org/10.1029/98JD00156>, 1998.](#)

903 [Willis, M. D., Leaitch, W. R., and Abbatt, J. P. D.: Processes Controlling the Composition and Abundance](#)
904 [of Arctic Aerosol, *Rev. Geophys.*, 56, 621–671, <https://doi.org/10.1029/2018RG000602>, 2018.](#)

905 [World Meteorological Organization \(WMO\): WMO/GAW aerosol measurement procedures, guidelines](#)
906 [and recommendations, WMO, Geneva, 2003.](#)

907 [Yang, X., Neděla, V., Ruňstuk, J., Ondrušková, G., Krausko, J., Vetráková, L., and Heger, D.: Evaporating](#)
908 [brine from frost flowers with electron microscopy and implications for atmospheric chemistry and sea-](#)
909 [salt aerosol formation, *Atmospheric Chem. Phys.*, 17, 6291–6303, \[https://doi.org/10.5194/acp-17-6291-\]\(https://doi.org/10.5194/acp-17-6291-2017\)](#)
910 [2017](#), 2017.

911 [Zhang, L., Gong, S., Padro, J., and Barrie, L.: A size-segregated particle dry deposition scheme for an](#)
912 [atmospheric aerosol module, *Atmos. Environ.*, 35, 549–560, 2001.](#)

913 [Abbatt, J. P. D., Thomas, J. L., Abrahamsson, K., Boxe, C., Granfors, A., Jones, A. E., King, M. D., Saiz Lopez,](#)
914 [A., Shepson, P. B., Sodeau, J., Toohey, D. W., Toubin, C., Von Glasow, R., Wren, S. N., and Yang, X.: Halogen](#)
915 [activation via interactions with environmental ice and snow in the polar lower troposphere and other](#)
916 [regions, *Atmospheric Chem. Phys.*, 12, 6237–6271, <https://doi.org/10.5194/acp-12-6237-2012>, 2012.](#)

917 [Alvarez Aviles, L., Simpson, W. R., Douglas, T. A., Sturm, M., Perovich, D., and Domine, F.: Frost flower](#)
918 [chemical composition during growth and its implications for aerosol production and bromine activation,](#)
919 [*J. Geophys. Res. Atmospheres*, 113, 2008JD010277, <https://doi.org/10.1029/2008JD010277>, 2008.](#)

920 [Amos, H. M., Jacob, D. J., Holmes, C. D., Fisher, J. A., Wang, Q., Yantosca, R. M., Corbitt, E. S., Galarneau,](#)
921 [E., Rutter, A. P., Gustin, M. S., Steffen, A., Schauer, J. J., Graydon, J. A., Louis, V. L. St., Talbot, R. W., Edgerton,](#)
922 [E. S., Zhang, Y., and Sunderland, E. M.: Gas particle partitioning of atmospheric Hg\(II\) and its effect on](#)
923 [global mercury deposition, *Atmospheric Chem. Phys.*, 12, 591–603, \[https://doi.org/10.5194/acp-12-591-\]\(https://doi.org/10.5194/acp-12-591-2012\)](#)
924 [2012](#), 2012.

925 [Chen, Q., Mirrielees, J. A., Thanekar, S., Loeb, N. A., Kirpes, R. M., Upchurch, L. M., Barget, A. J., Lata, N.,](#)
926 [N., Raso, A. R. W., McNamara, S. M., China, S., Quinn, P. K., Ault, A. P., Kennedy, A., Shepson, P. B., Fuentes,](#)

Formatted: Justified

927 J. D., and Pratt, K. A.: Atmospheric particle abundance and sea salt aerosol observations in the springtime
928 Arctic: a focus on blowing snow and leads, *Atmospheric Chem. Phys.*, **22**, 15263–15285,
929 <https://doi.org/10.5194/acp-22-15263-2022>, 2022.

930 Community, T. I. G. C. U.: *geoschem/GCClassic: GEOS-Chem 13.2.1*,
931 <https://doi.org/10.5281/ZENODO.5500717>, 2021.

932 Confer, K. L., Jaeglé, L., Liston, G. E., Sharma, S., Nandan, V., Yackel, J., Ewert, M., and Horowitz, H. M.:
933 Impact of Changing Arctic Sea Ice Extent, Sea Ice Age, and Snow Depth on Sea Salt Aerosol From Blowing
934 Snow and the Open Ocean for 1980–2017, *J. Geophys. Res. Atmospheres*, **128**, e2022JD037667,
935 <https://doi.org/10.1029/2022JD037667>, 2023.

936 Cox, C. J., Walden, V. P., Rowe, P. M., and Shupe, M. D.: Humidity trends imply increased sensitivity to
937 clouds in a warming Arctic, *Nat. Commun.*, **6**, 10117, <https://doi.org/10.1038/ncomms10117>, 2015.

938 DeMott, P. J., Hill, T. C. J., McCluskey, C. S., Prather, K. A., Collins, D. B., Sullivan, R. C., Ruppel, M. J., Mason,
939 R. H., Irish, V. E., Lee, T., Hwang, C. Y., Rhee, T. S., Snider, J. R., McMeeking, G. R., Dhaniyala, S., Lewis, E. R.,
940 Wentzell, J. J. B., Abbatt, J., Lee, C., Sultana, C. M., Ault, A. P., Axson, J. L., Diaz-Martinez, M., Venero, I.,
941 Santos-Figueroa, G., Stokes, M. D., Deane, G. B., Mayol-Bracero, O. L., Grassian, V. H., Bertram, T. H.,
942 Bertram, A. K., Moffett, B. F., and Franc, G. D.: Sea spray aerosol as a unique source of ice nucleating
943 particles, *Proc. Natl. Acad. Sci.*, **113**, 5797–5803, <https://doi.org/10.1073/pnas.1514034112>, 2016.

944 Dibb, J. E., Ziemba, L. D., Luxford, J., and Beckman, P.: Bromide and other ions in the snow, firn air, and
945 atmospheric boundary layer at Summit during GSHOX, *Atmospheric Chem. Phys.*, **10**, 9931–9942,
946 <https://doi.org/10.5194/acp-10-9931-2010>, 2010.

947 Freud, E., Krejci, R., Tunved, P., Leaitch, R., Nguyen, Q. T., Massling, A., Skov, H., and Barrie, L.: Pan-Arctic
948 aerosol number size distributions: seasonality and transport patterns, *Atmospheric Chem. Phys.*, **17**, 8101–
949 8128, <https://doi.org/10.5194/acp-17-8101-2017>, 2017.

950 Gelaro, R., McCarty, W., Suárez, M. J., Todling, R., Molod, A., Takacs, L., Randles, C. A., Darmenov, A.,
951 Bosilovich, M. G., Reichle, R., Wargan, K., Coy, L., Cullather, R., Draper, C., Akella, S., Buchard, V., Conaty,
952 A., Da Silva, A. M., Gu, W., Kim, G. K., Koster, R., Lucchesi, R., Merkova, D., Nielsen, J. E., Partyka, G.,
953 Pawson, S., Putman, W., Rienecker, M., Schubert, S. D., Sienkiewicz, M., and Zhao, B.: The Modern-Era
954 Retrospective Analysis for Research and Applications, Version 2 (MERRA 2), *J. Clim.*, **30**, 5419–5454,
955 <https://doi.org/10.1175/JCLI-D-16-0758.1>, 2017.

956 Gong, S. L.: A parameterization of sea salt aerosol source function for sub- and super-micron particles,
957 *Glob. Biogeochem. Cycles*, **17**, 2003GB002079, <https://doi.org/10.1029/2003GB002079>, 2003.

958 Held, A., Brooks, I. M., Leck, C., and Tjernström, M.: On the potential contribution of open lead particle
959 emissions to the central Arctic aerosol concentration, *Atmospheric Chem. Phys.*, **11**, 3093–3105,
960 <https://doi.org/10.5194/acp-11-3093-2011>, 2011.

961 Hoffman, J. P., Ackerman, S. A., Liu, Y., and Key, J. R.: A 20-Year Climatology of Sea Ice Leads Detected in
962 Infrared Satellite Imagery Using a Convolutional Neural Network, *Remote Sens.*, **14**, 5763,
963 <https://doi.org/10.3390/rs14225763>, 2022.

964 Huang, J. and Jaeglé, L.: Wintertime enhancements of sea salt aerosol in polar regions consistent with a
965 sea ice source from blowing snow, *Atmospheric Chem. Phys.*, **17**, 3699–3712,
966 <https://doi.org/10.5194/acp-17-3699-2017>, 2017.

967 Huang, J., Jaeglé, L., and Shah, V.: Using CALIOP to constrain blowing snow emissions of sea salt aerosols
968 over Arctic and Antarctic sea ice, *Atmospheric Chem. Phys.*, **18**, 16253–16269,
969 <https://doi.org/10.5194/acp-18-16253-2018>, 2018.

970 Huang, J., Jaeglé, L., Chen, Q., Alexander, B., Sherwen, T., Evans, M. J., Theys, N., and Choi, S.: Evaluating
971 the impact of blowing snow sea salt aerosol on springtime BrO and O₃ in the
972 Arctic, *Atmospheric Chem. Phys.*, **20**, 7335–7358, <https://doi.org/10.5194/acp-20-7335-2020>, 2020.

973 Integrated Climate Data Center (ICDC), CEN, and University of Hamburg, Hamburg, Germany: AMSR-E
974 Arctic lead area fraction, n.d.

975 Intergovernmental Panel On Climate Change: Climate Change 2021 – The Physical Science Basis: Working
976 Group I Contribution to the Sixth Assessment Report of the Intergovernmental Panel on Climate Change,
977 1st ed., Cambridge University Press, <https://doi.org/10.1017/9781009157896>, 2023.

978 Ioannidis, E., Law, K. S., Raut, J. C., Marelle, L., Onishi, T., Kirpes, R. M., Upchurch, L., Massling, A., Skov, H.,
979 Quinn, P. K., and Pratt, K. A.: Modelling wintertime Arctic Haze and sea spray aerosols,
980 *Aerosols/Atmospheric Modelling and Data Analysis/Troposphere/Chemistry (chemical composition and
981 reactions)*, <https://doi.org/10.5194/egusphere-2022-310>, 2022.

982 Jaeglé, L., Quinn, P. K., Bates, T. S., Alexander, B., and Lin, J. T.: Global distribution of sea salt aerosols: new
983 constraints from in situ and remote sensing observations, *Atmospheric Chem. Phys.*, **11**, 3137–3157,
984 <https://doi.org/10.5194/acp-11-3137-2011>, 2011.

985 Keller, C. A., Long, M. S., Yantosca, R. M., Da Silva, A. M., Pawson, S., and Jacob, D. J.: HEMCO v1.0: a
986 versatile, ESMF-compliant component for calculating emissions in atmospheric models, *Geosci. Model
987 Dev.*, **7**, 1409–1417, <https://doi.org/10.5194/gmd-7-1409-2014>, 2014.

988 Kirpes, R. M., Bonanno, D., May, N. W., Fraund, M., Barget, A. J., Moffet, R. C., Ault, A. P., and Pratt, K. A.:
989 Wintertime Arctic Sea Spray Aerosol Composition Controlled by Sea Ice Lead Microbiology, *ACS Cent. Sci.*,
990 **5**, 1760–1767, <https://doi.org/10.1021/acscentsci.9b00541>, 2019.

991 Leaitch, W. R., Russell, L. M., Liu, J., Kolonjari, F., Toom, D., Huang, L., Sharma, S., Chivulescu, A., Veber, D.,
992 and Zhang, W.: Organic functional groups in the submicron aerosol at 82.5° N, 62.5° W from 2012 to 2014,
993 *Atmospheric Chem. Phys.*, **18**, 3269–3287, <https://doi.org/10.5194/acp-18-3269-2018>, 2018.

994 Li, M., Liu, J., Qu, M., Zhang, Z., and Liang, X.: An Analysis of Arctic Sea Ice Leads Retrieved from AMSR-
995 E/AMSR2, *Remote Sens.*, **14**, 969, <https://doi.org/10.3390/rs14040969>, 2022.

996 Lin, H., Jacob, D. J., Lundgren, E. W., Sulprizio, M. P., Keller, C. A., Fritz, T. M., Eastham, S. D., Emmons, L. K.,
997 Campbell, P. C., Baker, B., Saylor, R. D., and Montuoro, R.: Harmonized Emissions Component (HEMCO) 3.0
998 as a versatile emissions component for atmospheric models: application in the GEOS-Chem, NASA GEOS,
999 WRF-GC, CESM2, NOAA-GEFS Aerosol, and NOAA-UFS models, *Geosci. Model Dev.*, **14**, 5487–5506,
1000 <https://doi.org/10.5194/gmd-14-5487-2021>, 2021.

1001 Liu, H., Jacob, D. J., Bey, I., and Yantosca, R. M.: Constraints from ^{210}Pb and ^7Be on wet deposition and
1002 transport in a global three-dimensional chemical tracer model driven by assimilated meteorological fields,
1003 *J. Geophys. Res. Atmospheres*, **106**, 12109–12128, <https://doi.org/10.1029/2000JD900839>, 2001.

1004 Luo, G. and Yu, F.: Impact of Air Refreshing and Cloud Ice Uptake Limitations on Vertical Profiles and Wet
1005 Depositions of Nitrate, Ammonium, and Sulfate, *Geophys. Res. Lett.*, **50**, e2023GL104258,
1006 <https://doi.org/10.1029/2023GL104258>, 2023.

1007 Luo, G., Yu, F., and Moch, J. M.: Further improvement of wet process treatments in GEOS-Chem v12.6.0:
1008 impact on global distributions of aerosols and aerosol precursors, *Geosci. Model Dev.*, **13**, 2879–2903,
1009 <https://doi.org/10.5194/gmd-13-2879-2020>, 2020.

1010 May, N. W., Quinn, P. K., McNamara, S. M., and Pratt, K. A.: Multiyear study of the dependence of sea salt
1011 aerosol on wind speed and sea ice conditions in the coastal Arctic, *J. Geophys. Res. Atmospheres*, **121**,
1012 9208–9219, <https://doi.org/10.1002/2016JD025273>, 2016.

1013 Monahan, E. C., Spiel, D. E., and Davidson, K. L.: A Model of Marine Aerosol Generation Via Whitecaps and
1014 Wave Disruption, in: *Oceanic Whitecaps*, vol. 2, edited by: Monahan, E. C. and Niocaill, G. M., Springer
1015 Netherlands, Dordrecht, 167–174, https://doi.org/10.1007/978-94-009-4668-2_16, 1986.

1016 Nilsson, E. D., Rannik, Ü., Swietlicki, E., Leck, C., Aalto, P. P., Zhou, J., and Norman, M.: Turbulent aerosol
1017 fluxes over the Arctic Ocean: 2. Wind driven sources from the sea, *J. Geophys. Res. Atmospheres*, **106**,
1018 32139–32154, <https://doi.org/10.1029/2000JD900747>, 2001.

1019 Pierce, J. R. and Adams, P. J.: Global evaluation of CCN formation by direct emission of sea salt and growth
1020 of ultrafine sea salt, *J. Geophys. Res. Atmospheres*, **111**, 2005JD006186,
1021 <https://doi.org/10.1029/2005JD006186>, 2006.

1022 Pound, R. J., Sherwen, T., Helmig, D., Carpenter, L. J., and Evans, M. J.: Influences of oceanic ozone
1023 deposition on tropospheric photochemistry, *Atmospheric Chem. Phys.*, **20**, 4227–4239,
1024 <https://doi.org/10.5194/acp-20-4227-2020>, 2020.

1025 Pratt, K. A., Custard, K. D., Shepson, P. B., Douglas, T. A., Pöhler, D., General, S., Zielcke, J., Simpson, W. R.,
1026 Platt, U., Tanner, D. J., Gregory Huey, L., Carlsen, M., and Stirm, B. H.: Photochemical production of
1027 molecular bromine in Arctic surface snowpacks, *Nat. Geosci.*, **6**, 351–356,
1028 <https://doi.org/10.1038/ngeo1779>, 2013.

1029 Quinn, P. K., Coffman, D. J., Kapustin, V. N., Bates, T. S., and Covert, D. S.: Aerosol optical properties in the
1030 marine boundary layer during the First Aerosol Characterization Experiment (ACE 1) and the underlying
1031 chemical and physical aerosol properties, *J. Geophys. Res.*, **103**, 16,547–16,563, 1998.

1032 Quinn, P. K., Bates, T. S., Miller, T. L., Coffman, D. J., Johnson, J. E., Harris, J. M., Ogren, J. A., Forbes, G.,
1033 Anderson, T. L., Covert, D. S., and Rood, M. J.: Surface submicron aerosol chemical composition: What
1034 fraction is not sulfate?, *J. Geophys. Res. Atmospheres*, **105**, 6785–6805,
1035 <https://doi.org/10.1029/1999JD901034>, 2000.

1036 Quinn, P. K., Miller, T. L., Bates, T. S., Ogren, J. A., Andrews, E., and Shaw, G. E.: A 3-year record of
1037 simultaneously measured aerosol chemical and optical properties at Barrow, Alaska, *J. Geophys. Res.*
1038 *Atmospheres*, **107**, <https://doi.org/10.1029/2001JD001248>, 2002.

1039 Radke, L. F., Hobbs, P. V., and Pinnons, J. E.: Observations of Cloud Condensation Nuclei, Sodium-Containing
1040 Particles, Ice Nuclei and the Light Scattering Coefficient Near Barrow, Alaska, *J. Appl. Meteor. Climatol.*, **15**,
1041 982–995, [https://doi.org/10.1175/1520-0450\(1976\)015%3C0982:OCCNS%3E2.0.CO;2](https://doi.org/10.1175/1520-0450(1976)015%3C0982:OCCNS%3E2.0.CO;2), 1976.

1042 Reiser, F., Willmes, S., and Heinemann, G.: A New Algorithm for Daily Sea Ice Lead Identification in the
1043 Arctic and Antarctic Winter from Thermal Infrared Satellite Imagery, *Remote Sens.*, **12**, 1957,
1044 <https://doi.org/10.3390/rs12121957>, 2020.

1045 Rhodes, R. H., Yang, X., Wolff, E. W., McConnell, J. R., and Frey, M. M.: Sea ice as a source of sea salt aerosol
1046 to Greenland ice cores: a model based study, *Atmospheric Chem. Phys.*, **17**, 9417–9433,
1047 <https://doi.org/10.5194/acp-17-9417-2017>.

1048 Riley, J. P. and Chester, R.: Introduction to marine chemistry, Academic Press, London, New York, 465 pp.,
1049 1971.

1050 Röhrs, J. and Kaleschke, L.: An algorithm to detect sea ice leads by using AMSR-E passive microwave
1051 imagery, *The Cryosphere*, **6**, 343–352, <https://doi.org/10.5194/tc-6-343-2012>.

1052 Roscoe, H. K., Brooks, B., Jackson, A. V., Smith, M. H., Walker, S. J., Obbard, R. W., and Wolff, E. W.: Frost
1053 flowers in the laboratory: Growth, characteristics, aerosol, and the underlying sea ice, *J. Geophys. Res.*,
1054 **116**, D12301, <https://doi.org/10.1029/2010JD015144>, 2011.

1055 Schmale, J., Zieger, P., and Ekman, A. M. L.: Aerosols in current and future Arctic climate, *Nat. Clim. Change*,
1056 **11**, 95–105, <https://doi.org/10.1038/s41558-020-00969-5>, 2021.

1057 Scott, W. D. and Levin, Z.: Open Channels in Sea Ice (Leads) as Ion Sources, *Science*, **177**, 425–426,
1058 <https://doi.org/10.1126/science.177.4047.425>, 1972.

1059 Simpson, W. R., Alvarez Aviles, L., Douglas, T. A., Sturm, M., and Domine, F.: Halogens in the coastal snow
1060 pack near Barrow, Alaska: Evidence for active bromine air snow chemistry during springtime, *Geophys.*
1061 *Res. Lett.*, **32**, 2004GL021748, <https://doi.org/10.1029/2004GL021748>, 2005.

1062 Simpson, W. R., Von Glasow, R., Riedel, K., Anderson, P., Ariya, P., Bottenheim, J., Burrows, J., Carpenter, L.
1063 J., Frieb, U., Goodsite, M. E., Heard, D., Hutterli, M., Jacobi, H. W., Kaleschke, L., Neff, B., Plane, J., Platt, U.,
1064 Richter, A., Roscoe, H., Sander, R., Shepson, P., Sodeau, J., Steffen, A., Wagner, T., and Wolff, E.: Halogens
1065 and their role in polar boundary layer ozone depletion, *Atmospheric Chem. Phys.*, **7**, 4375–4418,
1066 <https://doi.org/10.5194/acp-7-4375-2007>.

1067 Stramler, K., Del Genio, A. D., and Rossow, W. B.: Synoptically Driven Arctic Winter States, *J. Clim.*, **24**, 1747–
1068 1762, <https://doi.org/10.1175/2010JCLI3817.1>, 2011.

1069 Stutz, J., Thomas, J. L., Hurlock, S. C., Schneider, M., Von Glasow, R., Piot, M., Gorham, K., Burkhardt, J. F.,
1070 Ziemba, L., Dibb, J. E., and Lefer, B. L.: Longpath DOAS observations of surface BrO at Summit, Greenland,
1071 *Atmospheric Chem. Phys.*, **11**, 9899–9910, <https://doi.org/10.5194/acp-11-9899-2011>.

1072 Sumata, H., De Steur, L., Divine, D. V., Granskog, M. A., and Gerland, S.: Regime shift in Arctic Ocean sea
1073 ice thickness, *Nature*, **615**, 443–449, <https://doi.org/10.1038/s41586-022-05686-x>, 2023.

1074 Swanson, W. F., Holmes, C. D., Simpson, W. R., Confer, K., Marelle, L., Thomas, J. L., Jaeglé, L., Alexander,
1075 B., Zhai, S., Chen, Q., Wang, X., and Sherwen, T.: Comparison of model and ground observations finds
1076 snowpack and blowing snow aerosols both contribute to Arctic tropospheric reactive bromine,
1077 *Atmospheric Chem. Phys.*, **22**, 14467–14488, <https://doi.org/10.5194/acp-22-14467-2022>, 2022.

1078 Vaughan, D., Comiso, J., Allison, I., Carrasco, J., Kaser, G., Kwok, R., Mote, P., Murray, T., Paul, F., Ren, J. F.,
1079 Rignot, E., Solomina, O., Steffen, K., and Zhang, T.: Observations: Cryosphere, in: *Climate Change 2013: The*
1080 *Physical Science Basis*, 317–382, 2013.

1081 Wang, Q., Jacob, D. J., Spackman, J. R., Perring, A. E., Schwarz, J. P., Moteki, N., Marais, E. A., Ge, C., Wang,
1082 J., and Barrett, S. R. H.: Global budget and radiative forcing of black carbon aerosol: Constraints from pole-
1083 to pole (HIPPO) observations across the Pacific, *J. Geophys. Res. Atmospheres*, **119**, 195–206,
1084 <https://doi.org/10.1002/2013JD020824>, 2014.

1085 Wang, Q., Danilov, S., Jung, T., Kaleschke, L., and Wernecke, A.: Sea ice leads in the Arctic Ocean: Model
1086 assessment, interannual variability and trends, *Geophys. Res. Lett.*, **43**, 7019–7027,
1087 <https://doi.org/10.1002/2016GL068696>, 2016.

1088 Wang, X., Jacob, D. J., Downs, W., Zhai, S., Zhu, L., Shah, V., Holmes, C. D., Sherwen, T., Alexander, B., Evans,
1089 M. J., Eastham, S. D., Neuman, J. A., Veres, P. R., Koenig, T. K., Volkamer, R., Huey, L. G., Bannan, T. J.,
1090 Percival, C. J., Lee, B. H., and Thornton, J. A.: Global tropospheric halogen (Cl, Br, I) chemistry and its impact
1091 on oxidants, *Atmospheric Chem. Phys.*, **21**, 13973–13996, <https://doi.org/10.5194/acp-21-13973-2021>,
1092 2021.

1093 Wang, Y., Jacob, D. J., and Logan, J. A.: Global simulation of tropospheric O₃–NO_x–hydrocarbon chemistry:
1094 3. Origin of tropospheric ozone and effects of nonmethane hydrocarbons, *J. Geophys. Res. Atmospheres*,
1095 **103**, 10757–10767, <https://doi.org/10.1029/98JD00156>, 1998.

1096 Willis, M. D., Leaitch, W. R., and Abbatt, J. P. D.: Processes Controlling the Composition and Abundance of
1097 Arctic Aerosol, *Rev. Geophys.*, **56**, 621–671, <https://doi.org/10.1029/2018RG000602>, 2018.

1098 World Meteorological Organization (WMO): WMO/GAW aerosol measurement procedures, guidelines
1099 and recommendations, WMO, Geneva, 2003.

1100 Yang, X., Neděla, V., Runštuk, J., Ondrušková, G., Krausko, J., Vetráková, L., and Heger, D.: Evaporating brine
1101 from frost flowers with electron microscopy and implications for atmospheric chemistry and sea salt
1102 aerosol formation, *Atmospheric Chem. Phys.*, **17**, 6291–6303, <https://doi.org/10.5194/acp-17-6291-2017>,
1103 2017.

1104 Zhang, L., Gong, S., Padro, J., and Barrie, L.: A size-segregated particle dry deposition scheme for an
1105 atmospheric aerosol module, *Atmos. Environ.*, **35**, 549–560, 2001.

1106